

1 **Spatial and temporal evolution of future atmospheric**
2 **reactive nitrogen deposition in China under different climate**
3 **change mitigation strategies**

4 Mingrui Ma¹, Jiachen Cao^{2,3}, Dan Tong⁴, Bo Zheng⁵, Yu Zhao^{1,2*}

6 1. State Key Laboratory of Pollution Control and Resource Reuse and School of
7 Environment, Nanjing University, 163 Xianlin Rd., Nanjing, Jiangsu 210023, China.

8 2. Jiangsu Collaborative Innovation Center of Atmospheric Environment and
9 Equipment Technology (CICAEET), Nanjing University of Information Science and
10 Technology, Jiangsu 210044, China.

11 3. School of Environmental Science and Engineering, Nanjing University of
12 Information Science and Technology, Nanjing 210044, China.

13 4. Ministry of Education Key Laboratory for Earth System Modelling, Department of
14 Earth System Science, Tsinghua University, Beijing 100084, China

15 5. Institute of Environment and Ecology, Tsinghua Shenzhen International Graduate
16 School, Tsinghua University, Shenzhen 518055, China.

17
18
19 *Corresponding author: Yu Zhao

20 Phone: 86-25-89680650; email: yuzhao@nju.edu.cn

21

22 **Abstract**

23 Atmospheric reactive nitrogen (Nr) deposition plays a crucial role in linking air
24 pollution to ecosystem risks. Previous modeling studies have indicated that climate
25 change and pollution controls jointly result in significant changes in Nr deposition in
26 China. However, it remains unclear how future emission reductions will influence Nr
27 deposition under different climate pathways. Here, we investigated the spatiotemporal
28 evolution and driving factors of future Nr deposition under various national clean air
29 and climate policies. We applied WRF-CMAQ and assessed the historical (2010s,
30 2010-2014) pattern and future changes of Nr deposition till the 2060s (2060-2064) in
31 China, by combining two SSP-RCP global climate pathways and three national
32 emission control scenarios. The results show that the implementation of clean air and
33 carbon neutrality policies would greatly reduce oxidized nitrogen (OXN) deposition,
34 mitigate the adverse perturbations of climate change, and reduce the outflow from
35 Eastern China (EC) to West Pacific. In North China (NC), the weakened atmospheric
36 oxidation capacity (AOC) would elevate the response of OXN deposition to a 20%
37 abatement of emissions (expressed as the ratio of percentage change of deposition to
38 emissions) from 82.6% in the 2010s to nearly 100% in the 2060s. In contrast, the
39 response of **reduced nitrogen (RDN)** deposition to NH₃ emissions would decline, likely
40 attributable to a more NH₃-rich condition. The outcomes of this work broaden scientific
41 understanding on how anthropogenic actions of air quality improvement and carbon
42 emission reduction would reshape the future Nr deposition and support effective
43 policymaking to reduce associated ecological damages.

44 **Keywords:** Nr deposition, SSP-RCP, climate change, outflow pollution, emission
45 abatement

46

47 **1. Introduction**

48 With vigorous development of industrial and agricultural activities worldwide

49 since the industrial revolution, the emissions of reactive nitrogen (Nr, including
50 oxidized and reduced nitrogen species, OXN and RDN, respectively) have increased
51 explosively (Kanakidou et al., 2016), elevating the Nr levels in both atmosphere and
52 deposition. Enriched ambient Nr has led to a series of regional haze and ozone (O₃)
53 pollution issues through participation in atmospheric aerosol formation and
54 photochemical reactions (Chen et al., 2021). Furthermore, excessive atmospheric Nr
55 deposits onto land and water bodies through both dry and wet forms, directly hurting
56 the stability and productivity of the entire ecosystem (Flower et al., 2013). Substantial
57 Nr deposition can result in diverse adverse ecological effects, such as water
58 eutrophication (Zheng et al., 2020), soil acidification (Raza et al., 2020), and
59 biodiversity loss (Liu et al., 2017).

60 Influenced by multiple human activities, severe Nr deposition and its subsequent
61 ecological risks in China have attracted growing considerable attentions in recent years
62 (Gu et al., 2012; Liu and Du, 2020). China has undergone rapid industrialization and
63 urbanization, accompanied with explosive growth in the consumption of fossil fuels
64 and fertilizers over the past few decades, triggering significant emissions of NO_x and
65 NH₃ (Zhao et al. 2013; Kang et al. 2016). Enhanced Nr emissions made the country one
66 of the ~~hotpot~~hotspots receiving largest Nr deposition worldwide (Liu et al., 2013; Vet
67 et al., 2014). Observations of background sites from the China Nationwide Nitrogen
68 Deposition Monitoring Network (NNDMN) during 2011-2018 revealed that the annual
69 averaged Nr deposition fluxes reached 23.6 kg N ha⁻¹ yr⁻¹, vastly surpassing the
70 monitoring results in the United States (8.1 kg N ha⁻¹ yr⁻¹), Europe (8.7 kg N ha⁻¹ yr⁻¹)
71 and Japan (11.0 kg N ha⁻¹ yr⁻¹) (Wen et al., 2020).

72 EmployingDue to the fast change and heterogeneous distribution of emissions and
73 the typically short atmospheric lifetime of most Nr species, there exist challenges in
74 estimating the spatial pattern and long-term trend of Nr deposition across big countries
75 like China, based on observations at individual sites. Atmospheric chemistry transport
76 models (CTMs) or advanced statistical models —a support analyses of the interannual
77 variations of Nr deposition at multiple spatial scales (Liu et al., 2024; Wen et al., 2024).

78 A series of modeling studies have indicated that analyzed the magnitude and
79 spatiotemporal pattern of Nr deposition in China. Yu et al. (2019) applied the Kriging
80 interpolation combined with empirical remote sensing models and estimated that
81 China's annual Nr deposition had increased nearly 60% from 1980s to 2010s. By
82 developing a random forest algorithm, Zhou et al. (2023) quantified the considerable
83 growth of Nr deposition from 2005 to 2012 in eastern China. Gao et al. (2023) revealed
84 the shifting of deposition forms from dominated by wet to more balanced contributions
85 from dry and wet deposition. Nr deposition fluxes has increased nearly 60% since 1980s,
86 notably in eastern China (Gao et al., 2023, Yu et al. 2019, Zhao et al., 2022, Zhou et al.,
87 2023). Evidently, China is still struggling with serious Nr pollution. The national air
88 pollution control actions over the past decade have resulted in a fast decline in
89 emissions of acidic gaseous pollutants (mainly NO_x and SO₂) but relatively stable NH₃
90 (Zheng et al., 2018). The imbalance in emission reductions for different species has
91 altered the composition of Nr deposition, i.e.g., a growth in the proportion of RDN (Liu
92 et al., 2020). Zhao et al. (2022) developed the generalized additive model (GAM) and
93 found that the decline in OXN deposition lagged behind NO_x reductions in recent years,
94 attributed partly to the increased precipitation and the strengthening transport of
95 pollution. More importantly, the O₃ formation in eastern China has been primarily under
96 the NO_x-saturated condition, and the reduction in NO_x emissions, combined with
97 persistently high volatile organic compounds (VOCs) emissions, has enhanced the O₃
98 concentration and thereby the capacity of atmospheric oxidation. This has in turn
99 facilitated the conversion of NO_x to nitrate (NO₃⁻), and thus weakened the response of
100 OXN deposition to NO_x emission abatement, the increasingly strong capacity of
101 atmospheric oxidation, attributed primarily to the persistently high emissions of volatile
102 organic compounds (VOCs), has been weakening the response of OXN deposition to
103 NO_x emissions in eastern part of China and thus preventing effective reduction of Nr
104 deposition. One-unit abatement of NO_x emissions resulted in only less than 80%
105 abatement of OXN deposition, emphasizing the crucial role of active O₃-VOCs-NO_x
106 photochemistry in modulating the Nr deposition (Liu et al., 2022).

107 Atmospheric Nr deposition ~~are~~ is mainly influenced by rainfall, precursor emissions,
108 and long-distance transport (Ellis et al., 2013, Kim et al., 2012, Ma et al., 2023, Zhu et
109 al., 2022). ~~Future climate change may strengthen the local turbulence and precipitation~~
110 ~~intensity, which will alter the dry and wet deposition rate, respectively (Toyota et al.,~~
111 ~~2016; Xia et al., 2024). Meanwhile, the anticipated substantial reduction in Nr~~
112 ~~emissions through pollution controls will reduce the Nr deposition and change its~~
113 ~~dominant components~~~~The strengthening climate change and implementation of~~
114 ~~pollution controls will greatly alter the regional meteorological conditions and air~~
115 ~~pollutant emissions, resulting in substantial changes in magnitude and spatiotemporal~~
116 ~~pattern of Nr deposition.~~ The changing deposition will further exert multiple impacts
117 on the biodiversity, carbon sequestration and greenhouse emissions of various
118 ecosystems, and thus influence the climate and ecological environment profoundly
119 (Zhu et al., 2020). There are only a few studies addressing future Nr deposition in China.
120 They commonly employed coupled climate-chemistry global models to conduct
121 simulations under different predefined greenhouse gas (GHG) emission scenarios.
122 ~~Future emissions were primarily referencing the Intergovernmental Panel on Climate~~
123 ~~Change (IPCC)~~~~For example, a~~ A pioneering study by Galloway et al. (2004) predicted
124 significant growth in Nr deposition in East Asia, exceeding 50 kg N ha⁻¹ year⁻¹ yr⁻¹ by
125 2050, based on the Intergovernmental Panel on Climate Change IS92a (IPCC92a)
126 emission scenario. ~~The~~The Atmospheric Chemistry and Climate Model
127 Intercomparison Project (ACCMIP) presented a multi-model global ~~datasets~~dataset of
128 Nr deposition, ~~covering the period~~ from 1850 to 2100 (Lamarque et al. 2013a), with the
129 f-uture emissions obtained from the IPCC Representative Concentration Pathways
130 (RCPs) based on the radiative forcing in 2100 (van Vuuren et al., 2011). The Nr
131 deposition in East Asia was estimated to increase 27% and 39% in the 2030s under the
132 RCP2.6 and RCP8.5 ~~pathways~~, respectively (Lamarque et al. 2013b). ~~More~~
133 ~~recently~~Based on ACCMIP datasets, Zhang et al. (2019) ~~and Sun et al. (2022)~~ reported
134 ~~that the possible future changes in OXN and RDN deposition, respectively, based on~~
135 ~~ACCMIP datasets.~~ The OXN deposition fluxes under both RCP4.5 and RCP8.5

136 ~~pathways~~ were projected to increase in 2030s but decrease by the end of the century,
137 driven primarily by the Nr emission trends. More recently, Sun et al. (2022) examined
138 the possible future changes in RDN deposition by combining ACCMIP datasets and
139 extra CMAQ simulations. The proportion of RDN in total deposition in eastern China
140 was projected to rise from 38% in 2000 to 56% in 2100 under RCP8.5 ~~pathway~~,
141 suggesting a transition in the dominant form from oxidized to reduced.

142 ~~Even While~~ previous studies ~~made insightful predictions on~~ have provided valuable
143 information on the future evolution of Nr deposition in China, they have insufficiently
144 ~~incorporated~~ considered the impact of the potentially profound emission reduction
145 resulting from implementation of climate and pollution control policies in the context
146 ~~of global climate change.~~ In 2020, China announced the plan to achieve carbon
147 neutrality by 2060, and the effects of a wide range of sharp emission reductions on
148 future environment has become a major research focus (Dong et al., 2021). Researchers
149 have integrated national strategies of emission reduction to assess future air pollution
150 and associated health risks in China under various climate change pathways (Cheng et
151 al., 2021a, Cheng et al., 2023, Shi et al., 2021). For example, the IPCC Sixth
152 Assessment Report (AR6) introduced a scientifically combined set of pathways known
153 as Shared Socioeconomic Pathways (SSPs) and RCPs, denoted as SSP-RCP (IPCC,
154 2021). New pathways integrate the impact of socioeconomic development into the
155 framework for the evolution of GHG levels, offering more reliable projections of
156 possible outcomes of climate change (Cook et al., 2020; O'Neill et al., 2016, Xin et al.,
157 2020). However, there is a noticeable gap in assessment of China's atmospheric
158 deposition under the SSP-RCP framework. The roles of future emission and climate
159 changes on deposition remain unclear across diverse climate pathways. Moreover,
160 ~~stringent emission controls with diverse progresses for various species and regions~~ the
161 diverse trajectories of emission for various species and regions will change the
162 atmospheric oxidizing capacity and regional transport of pollution, respectively, which
163 will in turn change, and thereby alter the response of Nr deposition to the changing
164 precursor emission ~~emissions of their precursors.~~ ~~Given the crucial role of atmospheric~~

165 ~~deposition in connecting air pollution to ecosystem risks, it~~ is essential to evaluate
166 these anticipated changes for a comprehensive understanding of the ecological and
167 environmental impacts of Nr deposition, for aduring the long-term period with
168 continuous air pollution controls and~~progress of continuous air quality improvement~~
169 ~~and~~ global warming prevention.

170 In this study, we applied an air quality model (WRF-CMAQ, see details in methods)
171 and assessed the future changes of Nr deposition in China, by combining the SSP-RCP
172 global climate change pathways and the national emission control scenarios. The
173 historical period was chosen as 2010-2014, representing the years with the highest Nr
174 emissions in China, and the future simulation period was determined as 2060-2064.
175 Firstly, we evaluated the model performance of meteorology and Nr deposition for the
176 historical period based on available ground observations. We then quantified the spatial
177 and temporal changes of future Nr deposition and identified the main driving factors
178 under two IPCC pathways, SSP2-4.5 and SSP5-8.5). The SSP5-8.5 ~~pathway~~ represents
179 high GHG emissions characterized by continued reliance on fossil fuels, often viewed
180 as a pessimistic outlook for future climate change- (Alexandrov et al., 2021;
181 Meinshausen et al., 2020). Conversely, the SSP2-4.5 ~~pathway~~ envisions moderate GHG
182 emissions, achieved through the consideration of environmental policies and
183 technological advancements- (O'Neill et al., 2020; Su et al., 2021). We further assessed
184 the effects of various emissions abatement scenarios on Nr deposition. Finally, we
185 analyzed the future response of deposition to emission perturbation under different
186 scenarios. The study enhances scientific understanding on the interactions between
187 anthropogenic activities and atmospheric chemistry along with a changing climate, and
188 in turn supports the development of effective environmental policies to alleviate the
189 adverse effects of Nr pollution on ecosystems and human health.

2. Methodology and data

2.1 Model description and driving data

2.1.1 CMAQ model

The Community Multiscale Air Quality (CMAQ) model version 5.2 (available at <https://epa.gov/cmaq/access-cmaq-source-code>); Appel et al., 2017) was adopted to conduct atmospheric Nr deposition simulations over mainland China for both historical (2010-2014) and future periods (2060-2064). As a three-dimensional Eulerian model developed by the United States Environmental Protection Agency (USEPA), CMAQ comprehensively considers the complex atmospheric physical and chemical processes among various air pollutants, primarily including advection, vertical mixing, chemistry of gas and aerosol phase, cloud chemistry, as well as dry and wet deposition (Benish et al., 2022; Fahey et al., 2017). The model incorporates the temporal and spatial variations of chemical mechanisms, emissions and meteorology, thus effectively accounting for nonlinearity and regional transport (Liu et al., 2010). ~~To avoid the model errors associated with individual years, full-year simulations were conducted for every year of the two five-year intervals, and the five-year averages were used for further analyses. A series of simulation cases were designed by combining individual climate pathways and national emission scenarios to separate the roles of multiple factors on future deposition (see details in Section 2.2).~~ Developed by the United States Environmental Protection Agency (USEPA), CMAQ has been demonstrated to possess extensive practicality and sophistication in simulating regional air quality and acid deposition (Appel et al., 2017; Chang et al., 2020; Cheng et al., 2021; Liu et al., 2010). A single domain covering mainland China (186 × 156 grid cells) was adopted for the simulations with a horizontal resolution at 27 × 27 km per grid (Figure S1). Lambert conformal conic projection was applied for the domain centered at (102°E, 37°N) with two true latitudes, 40°N and 25°N. In the vertical direction, 30 eta levels with the pressure of 50hPa at the top level were used. For chemical configuration, the carbon

217 bond 05 (CB05) gas-phase chemical scheme and the AERO 6 aerosol scheme were
218 adopted (Sarwar et al., 2008, Pye et al., 2017, Murphy et al., 2017). The boundary
219 condition of trace gases used in this study was background concentration (default setup
220 in CMAQ model). To avoid the model errors associated with individual years, full-year
221 simulations were conducted for every year of the two five-year intervals, and the five-
222 year averages were used for further analyses. Simulation of each year included a one-
223 month spin-up time (i.e., 1st-31st December of the previous year) to reduce the impact
224 of the initial conditions on the simulations. A series of simulation cases were designed
225 by combining individual climate pathways and national emission scenarios to separate
226 the roles of multiple factors on future deposition (see details in Section 2.2).

227 2.1.2 Emissions input

228 The Multi-resolution Emission Inventory for China version 1.3 developed by
229 Tsinghua University (MEICv1.3, available at
230 http://www.meicmodel.org/?page_id=560; Li et al., 2017; Zheng et al., 2018) provided
231 historical anthropogenic emission data within China in our simulations. Information on
232 future emissions were obtained from the Dynamic Projection model for Emissions in
233 China version 1.1 developed by Tsinghua University (DPECv1.1, available at
234 http://meicmodel.org.cn/?page_id=1917); [Cheng et al., 2021a, 2021b](#)). DPEC links
235 global climate mitigation pathways to local clean air policies and fully incorporates
236 China's strict air pollution control progress since the implementation of the “Action
237 Plan of Air Pollution Prevention and Control” in 2013. It thus ~~corrects~~better depicts the
238 ~~erroneous~~-emission trends of China compared to the results in the sixth Coupled Model
239 Intercomparison Project (~~CMIP~~CMIP6) scenarios (Cheng et al., 2021b; Tong et al.,
240 2020). Three emission scenarios, named as “Baseline”, “Current-goal”, and “Neutral-
241 goal”, were used in this work (see the simulation case design in Section 2.2). The
242 “Baseline” depicts a high-emission scenario in the absence of climate and pollution
243 control policies, equivalent to the SSP5-8.5 climate pathway. The “Current-goal”
244 scenario is a combination that takes into account SSP2-4.5 climate pathway along with

245 existing pollution control policies in China. The “Neutral-goal” scenario integrates
246 China's 2060 carbon neutrality goal with the most stringent pollution control policies.
247 Details of the scenarios were described in Cheng et al. (2021b).

248 Anthropogenic emissions outside of China were taken from the Asian
249 anthropogenic emission inventory, named MIX, developed by the Model Inter-
250 Comparison Study for Asia (MICS-Asia) project (available at
251 http://meicmodel.org.cn/?page_id=1770; Li et al., 2017). Biogenic emissions were
252 calculated by the Model Emissions of Gases and Aerosols from Nature developed under
253 the Monitoring Atmospheric Composition and Climate project version 2.1
254 (MEGANv2.1; Guenther et al., 2012). The initial horizontal resolutions of both
255 emission inventories were $0.25^\circ \times 0.25^\circ$, and they were interpolated into our simulation
256 domain with the resolution of 27 km.

257 **2.1.3 Meteorological driving field**

258 The Weather Research and Forecasting (WRF) model version 3.9.1 (available at
259 https://www2.mmm.ucar.edu/wrf/users/wrf_files/wrfv3.9/updates-3.9.1.html);
260 [Skamarock et al., 2008](#)) was applied to provide meteorological fields for CMAQ.
261 Developed and maintained collaboratively by the National Center for Atmospheric
262 Research (NCAR) and the National Oceanic and Atmospheric Administration (NOAA),
263 WRF model has been recognized as a state-of-the-art regional weather model and
264 widely utilized in short-term weather forecasting and regional meteorological research
265 (Huang et al., 2020, ~~Skamarock et al., 2008~~, Wang et al., 2021). For our historical
266 meteorological simulation, the fifth generation of European Centre for Medium-Range
267 Weather Forecasts (ECMWF) reanalysis dataset, ERA5 (available at
268 [https://cds.climate.copernicus.eu/cdsapp#!/dataset/reanalysis-era5-single-](https://cds.climate.copernicus.eu/cdsapp#!/dataset/reanalysis-era5-single-levels?tab=form)
269 [levels?tab=form](https://cds.climate.copernicus.eu/cdsapp#!/dataset/reanalysis-era5-single-levels?tab=form)) was adopted as the initial and boundary field (Hersbach et al., 2020).
270 The temporal and spatial resolution was 6 hours and $0.25^\circ \times 0.25^\circ$, respectively. For
271 simulation of future period, it is ~~commonly practical~~common practice to employ
272 climate forecast results from global climate models (GCMs) as the initial and boundary

273 conditions. In this study, a global bias-corrected multi-model (BCMM) climatological
 274 dataset with a horizontal resolution of $1.25^{\circ} \times 1.25^{\circ}$ at 6-hour intervals (available at
 275 <https://www.scidb.cn/en/detail?dataSetId=791587189614968832#p2>) was adopted to
 276 drive WRF model for 2060-2064. The BCMM dataset was reconstructed from 18
 277 GCMs of the CMIP6, with corrections for climatological mean and interannual variance
 278 biases based on ERA5 data from 1979-2014, providing more reliable projections of
 279 long-term non-linear trends of multiple climate variables compared with original
 280 CMIP6 model outputs. Details of BCMM product were described at Xu et al. (2021).
 281 We employed Pseudo Global Warming (PGW) method (Kawase et al., 2013, Liu et al.,
 282 2021, Lauer et al., 2013, Taniguchi et al., 2020) for statistical dynamical downscaling.
 283 Specifically, future driving fields were forced with the ERA5 data from reference period
 284 (2010-2014) plus a climate perturbation (difference between the years 2060-2064 and
 285 2010-2014) calculated from BCMM results, as shown in Eq. (1) and Eq (2):

$$286 \quad WRF_{input2060-2064} = ERA5_{2010-2014} + \Delta BCMM_{SSP} \quad (1)$$

$$287 \quad \Delta BCMM_{SSP} = BCMM_{\overline{2060-2064}} - BCMM_{\overline{2010-2014}} \quad (2)$$

288 where $\Delta BCMM_{SSP}$ is the CMIP6 multimodel ensemble mean change signal for 2060-
 289 2064 relative to 2010-2014 under the SSP2-4.5 or SSP5-8.5 pathway, $BCMM_{\overline{2060-2064}}$
 290 and $BCMM_{\overline{2010-2014}}$ represent the 5-year meteorological averages of BCMM dataset
 291 in the future and reference periods, respectively. Nine physical variables were perturbed
 292 in this study including zonal wind, meridional wind, air temperature, sea surface
 293 temperature, soil temperature, specific humidity, the surface pressure, sea-level
 294 pressure and geopotential height. The bilinear interpolation was applied to interpolate
 295 BCMM data to the ERA5 grid.

296 The land-use and land-cover (LULC) data were taken from global data of the U.S.
 297 Geological Survey (USGS) (de Meij et al., 2014; Pineda et al., 2004). The physical
 298 parameterization schemes used in all simulations are summarized in Table S1 in the
 299 Supplement.

2.1.4 Deposition mechanisms

The dry deposition (DDEP) of each atmospheric chemical species (i) was calculated as the product of surface concentration ($C^{surface}$) and dry deposition velocity (V_d) at the lowest model layer, as shown in Eq. (3):

$$DDEP_i = C_i^{surface} \times V_d \quad (3)$$

According to the classical resistance cascade model (Venkatram and Pleim, 1999; Wesely, 2007), the parameters of V_d are calculated as Eq. (4):

$$V_d = 1/(R_a + R_b + R_c) \quad (4)$$

where R_a is the aerodynamic resistance to the transfer from lowest layer to the roughness height, calculated as a function of surface layer turbulence parameters including friction velocity and the Monin-Obukhov length; R_b is the boundary layer resistance to transfer between the roughness height and surface; R_c is the resistance to surface uptake, which can be further divided into several series and parallel components, representing the resistance to the lower vegetation canopy or ground.

The algorithm module for wet deposition (WDEP) is derived from the regional acid deposition model (RADM; Chang et al., 1987) and depends on the precipitation rate (P_r) and cloud water concentration (C_{cloud}) of specific chemical component:

$$WDEP_i = P_r \cdot \bar{C}_i^{cloud} \quad (5)$$

The wet scavenging is considered in two pathways, depending upon whether the pollutant participates in the cloud water chemistry and on the liquid water content.

Details on how CMAQ removes pollutants through wet deposition can be found in the official CMAQ Science Documentation (available at https://www.cmascenter.org/cmaq/science_documentation/pdf/ch11.pdf). In this study,

OXN included NO, NO₂, HNO₃, N₂O₅, HONO, and particulates as nitrate (NO₃⁻)₅⁻, and RDN included NH₃ and particulates as ammonium (NH₄⁺).

2.2 Numerical simulation experiment design

To evaluate future changes in the spatiotemporal pattern of atmospheric Nr

327 deposition under different SSP-RCP climate pathways and emission control scenarios,
328 we performed parallel numerical simulation experiments with WRF-CMAQ, as
329 summarized in Table 1. Base case simulated the real situation in historical period (2010-
330 2014). Case 1 and Case 2 were designed to predict the atmospheric Nr deposition in the
331 2060s, following SSP2-4.5 climate pathway with “Current-goal” emission scenario in
332 DPEC and SSP5-8.5 climate pathway with “Baseline” emission scenario, respectively.
333 Difference between Case 1 and Base case and that between Case 2 and Base case
334 respectively revealed the changing Nr deposition from 2010s to 2060s in SSP2-4.5 and
335 SSP5-8.5.

336 Cases 3 and 4 applied future climate pathways (SSP2-4.5 and SSP5-8.5,
337 respectively) but historical emissions, and the difference between each of them and
338 Base case revealed how climate change would influence Nr deposition under
339 corresponding climate pathway. Meanwhile, the effect of emission change on future Nr
340 deposition was examined by comparing Case 3 and Case 1 for “Current-goal” scenario
341 in DPEC, and by comparing Case 4 and Case 2 for “Baseline” scenario. Case 5 applied
342 SSP2-4.5 climate pathway and “Neutral-goal” emission scenario in DPEC. Comparison
343 between Case 5 and Case 3 revealed the benefit of national emission controls under
344 China’s carbon neutrality policy on Nr deposition.

345 Cases 6-8 were designed based on Cases 1, ~~32~~, and 5, respectively. In these cases,
346 emissions in eastern China (EC) were set at the 2060s level, while those in western
347 China (WC) were maintained at the 2010s level. The aim was to explore the effect of
348 diverse emission control progresses for different regions on the future Nr deposition.
349 WC and EC were divided by longitude 110° east in this study, as shown in Figure S1.
350 In Cases 9-12, the emissions of all species were reduced by 20% from those in Cases 3,
351 1, 2, and 5, respectively, to explore the response of deposition to emission perturbation
352 at different atmospheric conditions caused by varying pollution control levels. The 20%
353 emissions reduction was regarded as a reasonable perturbation to achieve a significant
354 change (Galmarini et al., 2017).

2.3 Observations and model evaluation

WRF-CMAQ model performance was evaluated against available observation of meteorological variables and Nr deposition at monthly or annual level. Daily near-surface observations of four meteorological parameters including temperature at the height of 2 m (T2), relative humidity (RH), wind speed at the height of 10 m (WS10) and accumulated precipitation (PREC) were derived from the National Meteorological Data Center of China Meteorological Administration (CMA, <http://data.cma.cn/data/detail/dataCode/A.0012.0001.html>). The 839 meteorological surface stations, with continuous five-year observations from 2010 to 2014 were selected, as shown in Figure 1. Meanwhile, the monthly observations of Nr deposition fluxes were taken from the Nationwide Nitrogen Deposition Monitoring Network (NNDMN; Xu et al., 2018; 2019). ~~Following our previous study, we~~ We selected 28 sites for dry deposition fluxes and 53 sites for wet deposition fluxes, for which at least two-year continuous measurement data were available, to evaluate model performance. Details of monitoring stations can be found in ~~our previous study~~ (Ma et al., 2023). ~~As shown in Eq. (S1) and Eq (S2) in the supplement, the mean bias (MB) and mean error (ME), were used to evaluate the deviation level of meteorological parameter simulations.~~ Statistical indicators ~~for Nr deposition~~ were calculated with Eq. (6-9), including normalized mean bias (NMB), normalized mean error (NME) and the correlation coefficient (R) at temporal and spatial scales (Baker et al., 2004; Ma et al., 2023):

$$NMB = \sum_{i=1}^n (S_i - O_i) / \sum_{i=1}^n O_i \times 100\% \quad (6)$$

$$NME = \sum_{i=1}^n |S_i - O_i| / \sum_{i=1}^n O_i \times 100\% \quad (7)$$

$$R(\text{temporal}) = \sum_{i=1}^n (S_i - \bar{S})(O_i - \bar{O}) / \sqrt{\sum_{i=1}^n (S_i - \bar{S})^2 (O_i - \bar{O})^2} \quad (8)$$

$$R(\text{spatial}) = \sum_{j=1}^m (\bar{S}_j - \bar{S}_j) (\bar{O}_j - \bar{O}_j) / \sqrt{\sum_{j=1}^m (S_j - \bar{S}_j)^2 (O_j - \bar{O}_j)^2} \quad (9)$$

where S and O are the monthly meteorological variables or annual Nr deposition from model simulation and observation, respectively; \bar{S} and \bar{O} are the monthly mean meteorological variables or annual deposition from model simulation and observation,

383 respectively; i means the individual month or year and j means the individual site.

384 **3. Results and discussion**

385 **3.1 Evaluation of model performance**

386 We compared the simulated near-surface temperature, wind speed, relative
387 humidity and accumulated precipitation with observations at the monthly level, as
388 shown in Figure 1. The model reasonably reproduced the spatial pattern of near-surface
389 temperature with the spatial R reaching 0.95 (Figure 1a). Overestimation was found in
390 the southeast and northwest of the country while underestimation over the Tibetan
391 Plateau. At the national scale, T2 was generally underestimated with the **NMBMB** and
392 **NMEME** calculated at $-7.76\%0.94\text{ }^{\circ}\text{C}$ and $+2.75\%,1.54\text{ }^{\circ}\text{C}$, respectively. In addition,
393 the temporal R reached 0.99, indicating the simulation was in good agreement with
394 observation at the monthly level. Unlike T2, due to the modeling biases in the
395 topographic effects and the underestimation of urban land use in USGS (Carvalho et
396 al., 2012; Liao et al., 2015), WS10 was overestimated with **NMBMB** calculated at
397 $33.13\%0.69\text{ m s}^{-1}$ at the national scale (Figure 1b). Such overestimation was also
398 reported in other studies (Liu et al., 2020, Shen et al., 2021, Zhu et al., 2022). RH is
399 slightly underestimated with **NMBMB** and **NMEME** calculated at -1.5803% and
400 $8.945.82\%$, respectively, while both spatial and temporal R were greater than 0.8
401 (Figure 1c). PREC was generally underestimated, with **NMBMB** and **NMEME** at -
402 $19.39\%14.06\text{ mm}$ and $39.15\%,28.47\text{ mm}$, respectively. A clear gradient from northwest
403 to southeast China was well captured, and the temporal and spatial R were 0.83 and
404 0.76, respectively (Figure 1d).

405 The comparison between the simulated and observed annual Nr deposition
406 averaged over 2010-2014 at the site level are provided by form (dry and wet) and
407 species (OXN and RDN) in Table 2. Nr deposition was underestimated for all cases.
408 The NMB and NME for the dry deposition of OXN (**OXN_DDEP_OXN**) were
409 calculated at -9.07% and 2434.76% , respectively, and the analogous numbers for RDN

410 (~~RDN_DDEP_RDN~~) were at -15.12% and 43.24%. The uncertainty in NH₃ emission
411 inventories was frequently recognized as an important factor contributing to the
412 underestimation (Ma et al., 2023, Chang et al., 2020, Shen et al., 2023). The limited
413 development of intensive livestock breeding and farming in China poses a considerable
414 challenge in acquiring sufficient activity data and accurate emission factors, leading to
415 underestimation of emissions with the “bottom-up” approach. Utilizing satellite
416 constraints, Zhang et al. (2018) estimated that the total NH₃ emissions in China may be
417 underestimated by nearly 40%. Due to lack of direct observation, additionally, the dry
418 deposition at NNDMN sites was calculated by multiplying the observed surface
419 concentrations with V_d simulated from GEOS-Chem (Bey et al., 2001; Xu et al., 2019).
420 Difference in the parameterization schemes for calculating V_d of given trace gases or
421 aerosols between CTMs could also introduce modest uncertainty for assessment of
422 OXN deposition (Wu et al., 2018; Chang et al., 2020). ~~Compared to dry deposition, The~~
423 ~~wet deposition of OXN and RDN (OXN_WDEP_OXN and RDN_WDEP_RDN) was~~
424 ~~simulated to be far lower than the) were also underestimated compared to~~ observations,
425 with the NMBs calculated at -28.76% and -17.86%, respectively. Part of the reason may
426 be underestimation of precipitation (Figure 1d-), ~~given the closely linear relationship~~
427 ~~between wet deposition and precipitation on an annual accumulation basis (Sahu et al.,~~
428 ~~2010; Zhang et al., 2019).~~ More importantly, most of wet deposition measured at
429 NNDMN sites was actually “bulk deposition”, which included both wet deposition and
430 a small fraction of dry deposition (Xu et al., 2015). Therefore, the bias from observation
431 also contributed to the inconsistency.

432 Project of the Model Inter-Comparison Study for Asia (MICS-Asia) phase III
433 reported the performances of Nr deposition simulation with multiple models over China,
434 with the overall NMBs and NMEs ranged -47% – 67% and 48% – 82% for OXN, and
435 -70% – -29% and 44% – 72% for RDN, respectively (Ge et al., 2020). The model
436 performance in our study was comparable to previous studies. In addition, both spatial
437 and temporal R were greater than 0.6 for each deposition form and species. ~~This~~
438 ~~indicates that our 5-year simulations effectively capture the interannual variability.~~

439 Overall, our simulations reasonably reproduced the observed Nr deposition in both
440 magnitude and spatiotemporal patterns.

441 **3.2 Evolution of Nr deposition and the roles of climate and emission** 442 **changes**

443 Table 3 summarizes the simulated atmospheric Nr deposition over historical (Base
444 case) and future periods under SSP2-4.5 (Case 1) and SSP5-8.5 pathways (Case 2). The
445 annual averaged Nr deposition for 2010-2014 was simulated at 14.7 kg N ha⁻¹ yr⁻¹ for
446 mainland China (Base case). The contribution of RDN to total deposition reached 52%,
447 which was in good agreement with the multiple-model ensemble mean value in the
448 MICS-Asia phase III project (Ge et al., 2020). The ratio of wet deposition to total
449 deposition was 0.54 in our simulation, also close to other CTM and nationwide
450 observation results (Ge et al., 2020, Xu et al., 2015, Zhao et al., 2017).

451 ~~Figure 2 Under the SSP2-4.5 pathway, total Nr deposition would decrease to 9.0~~
452 ~~kg N ha⁻¹ yr⁻¹ during 2060-2064, primarily attributed to a sharp decline in OXN~~
453 ~~deposition (Case 1). Accompanied with an active energy transition and effective control~~
454 ~~of fossil fuel consumption, the substantial reduction of anthropogenic NO_x emissions~~
455 ~~led to a 56% decline in OXN deposition compared to the reference period. Meanwhile,~~
456 ~~RDN deposition would be reduced by only 22%, resulting from a modest abatement of~~
457 ~~NH₃ emissions. Figure S2 in the supplement shows the changes of NO_x and NH₃~~
458 ~~emissions in 2060 relative to the historical period (2010-2014) in various scenarios, and~~
459 ~~Figure S3S2 in the supplement provides the annual emissions by sector. Large emission~~
460 ~~changes would occur mainly in the east of China. By 2060s, the national NO_x emissions~~
461 ~~would decline 55% (-15.1 Mt) and 89% (-24.5 Mt) under the “Current-goal” and~~
462 ~~“Neutral-goal” emission scenario. (Figure 2b-c). Such reductions would come mainly~~
463 ~~from power, industry and transportation sectors, driven by the predicted transition of~~
464 ~~energy structure (Figures S3a-b). Due to less improvement in agriculture management,~~
465 ~~the NH₃ emissions would decline much slower by 28% (-2.9 Mt) and 47% (-4.9 Mt)~~
466 ~~under in the two emission reduction scenarios. Under the SSP2-4.5 pathway, the total~~

467 Nr deposition would decrease to 9.0 kg N ha⁻¹ yr⁻¹ during 2060-2064, primarily
468 attributed to a sharp decline in OXN deposition (Case 1). Accompanied with an active
469 energy transition and effective control of fossil fuel consumption, the substantial
470 reduction of anthropogenic NO_x emissions led to a 56% decline in OXN deposition
471 compared to the reference period. Meanwhile, RDN deposition would be reduced by
472 only 22%, resulting from a modest abatement of NH₃ emissions. ~~Under the~~ SSP5-
473 8.5 pathway, the global economy would maintain rapid growth without sufficient
474 considerations for climate change. A high dependence on fossil fuels (especially coal)
475 for energy consumption would result in a nationwide growth of annual NO_x emissions
476 by 24% (6.5 Mt) from 2010s to 2060s (“Baseline” scenario in DPEC, Figure [S2a2a](#)),
477 and thereby elevate the total Nr deposition to 15.4 kg N ha⁻¹ yr⁻¹ (Case 2). The
478 proportions of OXN and RDN in future Nr deposition were anticipated to vary across
479 different SSP-RCP pathways. Under ~~the~~ SSP2-4.5 pathway, RDN was predicted to be
480 the dominant species of Nr deposition in the 2060s, with a proportion to the total
481 estimated at 66%. Under ~~the~~ SSP5-8.5 pathway, the proportion of OXN to total
482 deposition was expected to expand from 48% in the 2010s to 55% in the 2060s. In
483 addition, we further investigated the interannual variability in Nr deposition for
484 historical (Base case) and future periods under SSP2-4.5 (Case 1) and SSP5-8.5
485 pathways (Case 2), as shown in Figure S3 in the supplement. With the combined
486 influence of emissions and meteorological factors, the standard deviation (SD) of Nr
487 deposition for the period during 2010-2014 was 0.78 kg N ha⁻¹ yr⁻¹. In the future
488 simulations ~~For 2060-2064, the emissions in Case 1 and Case 2 were held constant from~~
489 ~~year to year., and t~~ The interannual variability in Nr deposition ~~during 2060-2064~~
490 ~~resulting~~ solely from meteorological fluctuations, leading to ~~with the SDs~~
491 ~~estimated at~~ values of 0.27 kg N ha⁻¹ yr⁻¹ and 0.45 kg N ha⁻¹ yr⁻¹, respectively.

492 In terms of spatial pattern, our simulations present clearly larger regional
493 difference in China compared to the global results of ACCMIP, owing to finer
494 simulation resolution and more detailed regional emission information. Figure [23](#)
495 illustrates the spatial distribution of Nr deposition in historical period and the future

496 changes under different SSP-RCP pathways. For 2010-2014, a clear gradient from west
497 to east was found for all deposition forms and species (Figures 2a3a-d), driven mainly
498 by the spatial distributions of NH₃ and NO_x emissions. Dry deposition of OXN
499 (OXN_DDEP_OXN) appeared mainly in eastern China, especially in the Beijing-
500 Tianjin-Hebei (BTH), Yangtze River Delta (YRD) and Pearl River Delta (PRD) regions
501 (see Figure S1 for the locations of these regions), resulting mainly from the large NO_x
502 emissions caused by active industrialization and urbanization. Hotspots of RDN dry
503 deposition (RDN_DDEP_RDN) appeared mainly in the North China Plain and the
504 Sichuan Basin (SCB) with intensive agricultural activities. Further influenced by
505 precipitation patterns, the southern areas experienced greater wet deposition compared
506 to the north, consistent with previous studies (Han et al., 2017; Zhao et al., 2017).
507 Influenced jointly by the substantial rainfall and local Nr emissions, in particular, SCB
508 was of the largest wet deposition for both OXN and RDN (OXN_WDEP_OXN and
509 RDN_WDEP_RDN).

510 The future OXN deposition would exhibit contrasting trends between the SSP2-
511 4.5 and SSP5-8.5 pathways. Compared to historical periods, both dry and wet forms
512 were predicted to decrease in the 2060s under the SSP2-4.5 pathway, with national
513 average reductions of 2.2 kg N ha⁻¹ yr⁻¹ and 1.8 kg N ha⁻¹ yr⁻¹, respectively. Relative
514 large declines would be found in their respective hotspots (Case 1-Base case, Figures
515 2e3e-f). In contrast, a growth of OXN deposition would appear under the SSP5-8.5
516 pathway, contributed mainly by wet deposition. The changes of dry deposition would
517 be limited within 1 kg N ha⁻¹ yr⁻¹ at the national level (Case 2-Base case, Figures 2i-
518 2j3i-j). For RDN deposition, there would be a nationwide decline in the 2060s under
519 SSP2-4.5 pathway (Case 1-Base case, Figures 2g3g-h). Large decline would be found
520 for wet deposition in the SCB and the surrounding area, with the maximum exceeding
521 10 kg N ha⁻¹ yr⁻¹. The changes under the SSP5-8.5 pathway would be small, with the
522 national average reduced by 0.1 and 0.5 kg N ha⁻¹ yr⁻¹ for dry and wet deposition,
523 respectively (Case 2-Base case, Figures 2k3k-l).

524 With Cases 3 and 4 included in the analyses, we further estimated the impacts of

525 climate and emission change on future total Nr deposition and compared them with the
526 joint impact (Figure 34). Under the SSP2-4.5-pathway, the national average difference
527 in Nr deposition due to changing emissions alone ($-5.48 \text{ kg N ha}^{-1} \text{ yr}^{-1}$, Figure 3b4b)
528 was closer to that from joint impacts ($-5.77 \text{ kg N ha}^{-1} \text{ yr}^{-1}$, Figure 3e4c), while the
529 difference caused by climate change alone was small ($-0.29 \text{ kg N ha}^{-1} \text{ yr}^{-1}$, Figure 3a4a).
530 Additionally, the spatial correlation (R) between the difference in deposition due to
531 emission change alone and that due to both factors would be 0.8997 (Figure 3b4b),
532 while it would be clearly smaller at 0.66 between those due to climate change alone and
533 both factors (Figure 3a4a). This indicates that the future long-term Nr deposition would
534 be primarily dominated by emission change. Under the SSP5-8.5-pathway, the total
535 amount of Nr deposition change at the national level would also be dominated by the
536 varying emissions. The emission change alone would lead to a growth of nationwide
537 deposition at $0.83 \text{ kg N ha}^{-1} \text{ yr}^{-1}$ (Figure 3e4e), 90% of the total growth ($0.92 \text{ kg N ha}^{-1}$
538 yr^{-1} , Figure 3f4f). However, the spatial pattern of deposition would be largely
539 modulated by climate change, with the spatial R between the deposition differences due
540 to climate change alone and both factors reaching 0.84 (Figure 3d4d). The value would
541 only be 0.55 between differences due to emission change alone and both factors (Figure
542 3e4e). In the southern BTH, for example, future climate change would elevate the
543 deposition by over $4 \text{ kg N ha}^{-1} \text{ yr}^{-1}$. By comparing the roles of emission and climate
544 changes in Nr deposition under different SSP-RCP pathways, our study emphasizes that
545 the rigorous implementation of emission controls in the future can effectively mitigate
546 the adverse perturbations of climate change.

547 **3.3 Varying effects of different emission changing patterns on Nr** 548 **deposition**

549 We further quantified the effects of emission controls on the deposition of different
550 Nr components (OXN and RDN) and compared them under various future emission
551 scenarios (“Baseline”, “Current-goal”, and “Neutral-goal”). As illustrated in Figure 45,
552 with an exception of OXN deposition in “Baseline” scenario which would increase 24%

553 (1.42 kg N ha⁻¹ yr⁻¹) from 2010s to 2060s, the national Nr deposition would commonly
554 decline for other cases, ranging from 5% to 85% (0.27-4.93 kg N ha⁻¹ yr⁻¹). In the
555 “Neutral-goal” scenario, in particular, the national average OXN deposition was
556 predicted to decline to 0.98 kg N ha⁻¹ yr⁻¹ by 2060s (Figure S4), accounting for only
557 17% of the total Nr deposition. This implies that the continuous and substantial
558 reduction in NO_x emissions, implemented as part of the national strategy to address
559 climate change and to improve air quality, would make RDN become the dominant
560 contributor to future Nr deposition. Spatial correlation between future emission change
561 and the resulting deposition change was estimated and summarized in Table S2 in the
562 supplement for different emission scenarios. Compared with OXN, the spatial change
563 in RDN deposition would be more consistent with that of precursor emissions, indicated
564 by a much higher R for RDN (0.67-0.72) than OXN (0.24-0.35). The discrepancy could
565 result from the stronger regional transport of NO_x, which comes largely from high-stack
566 sources (Ma et al., 2020).

567 Figure 56 compares the relative changes in future Nr deposition and precursor
568 emissions for WC and EC in different emission scenarios. Under the “Baseline”
569 scenario (Figure 5a6a), the OXN deposition in WC was predicted to increase 47% from
570 2010s to 2060s. This growth would be notably smaller than that of NO_x emissions
571 (81%), suggesting that a larger amount of OXN in WC would deposit to the east through
572 atmospheric transport. However, the transport might be weakened from WC to EC in
573 the “Current-goal” (Figure 5b6b) and “Neutral-goal” scenarios (Figure 5e6c), in which
574 the OXN deposition in WC would decline (46% and 85%, respectively) greater than
575 that of NO_x emissions (41% and 77%, respectively). Additional experiments were
576 conducted to quantify the impact of changing transport from WC on deposition in EC,
577 by keeping the emissions in WC at the 2010s levels (Cases 6-8). The fluxes crossing
578 110°E from west to east were calculated within the altitude from the surface to ~~10050~~
579 hpa and latitude from 20°N to 50°N. Compared to the cases where emissions in WC
580 were maintained at the 2010 levels, the outflow fluxes of OXN would change by 17.57
581 (Case 2-Case 7), -20.10 (Case 1-Case 6) and -37.12 kg N s⁻¹ (Case 5-Case 8) for

582 “Baseline”, “Current-goal” and “Neutral-goal” scenarios, respectively (Table S3).
583 Consequently, the OXN deposition in EC would change by 0.30 (2%), -0.28 (-5%), and
584 -0.51 kg N ha⁻¹ yr⁻¹ (-27%) from 2010s to 2060s due to the emission variation in WC
585 for different scenarios (Table 4). We further calculated the ratio of changes in OXN
586 outflow to changes in NO_x emissions ($\Delta T/\Delta E$) by combining the sensitivity simulation
587 cases with fixed WC emissions as 2010s. As shown in Figure 6a, $\Delta T/\Delta E$ is greater than
588 1 in WC under the baseline emission scenario, indicating that “efficacy” of eastward
589 transport of OXN would be enhanced. This resulted in a growing OXN deposition that
590 would greatly lag behind the growth of emissions. The meteorological conditions of
591 high wind speeds and low humidity in WC would hinder the conversion of aerosol NO₃⁻,
592 resulting in a high proportion of NO₂ in total OXN. Gaseous NO₂ usually has stronger
593 long-distance transport capability, thus contributing to the high transport efficacy of
594 OXN. Under the two emission reduction scenarios, the efficacy of eastward transport
595 of OXN would decrease ($\Delta T/\Delta E < 1$), resulting in a larger decline in deposition
596 compared to that in emissions. (Figure 6b and 6c).

597 The OXN deposition in EC was predicted to increase 13%, despite a 17% growth
598 in NO_x emissions under the “Baseline” scenario (Figure ~~5a~~6a). The additional
599 deposition loss may have been exported off-land through long-distance transport
600 processes. Zhao et al. (2017) demonstrated that 30% of China’s Nr emissions from
601 2008-2010 were transported to the China Sea Area of the Northwest Pacific. We
602 calculated the outflow fluxes of OXN from EC crossing 123°E within the altitude from
603 the surface to ~~100hpa~~50hpa and latitude from 20°N to 50°N (Table S4). Under the
604 “Baseline” scenario, the outflow fluxes from EC in 2060s would increase by ~~34.56 kg~~
605 ~~N s⁻¹~~19% compared to the case with the emissions maintained at the 2010s level. ~~(Case~~
606 ~~2-Case 4).~~ In contrast, the outflow fluxes under the scenarios of “Current-goal” and
607 “Neutral-goal” ~~scenarios~~ would respectively decline by ~~94.45 (Case 1-Case 3)~~49% and
608 ~~172.86 kg N s⁻¹ (Case 5-Case 3)~~89% attributable to the emission abatement in EC;
609 ~~making the relative changes in NO_x emissions and OXN deposition would be essentially~~
610 ~~equal~~. The result implies that effective implementation of China’s clean air and carbon

611 neutrality policies would definitely weaken its role of exporting pollution to west
612 Pacific. More importantly, compared to the declining transport efficacy of OXN from
613 WC to EC, with $\Delta T/\Delta E$ around 0.8, the $\Delta T/\Delta E$ in EC is closer to 1, indicating more
614 similar changes in NO_x emissions and OXN deposition. The disparity in transport
615 intensity between WC and EC leads to uneven changes in deposition and emissions,
616 highlighting the important role of inter-regional transport in the evolution of pollutant
617 source-sink relationships.

618 For RDN deposition, the relative change in emissions and deposition would be
619 essentially the same under the “Baseline” scenario (Figure 5a6a). However, the change
620 in RDN deposition would be smaller than that of NH_3 emissions for both EC and WC
621 in the remaining two scenarios (Figure 5b6b and 5e6c). Given its short atmospheric
622 lifetime (generally a few hours) and thereby limited long-distance transport capability
623 (Hertel et al., 2006), the lag in RDN deposition reduction could primarily result from
624 chemical transformation processes. As a crucial reduced gas in the atmosphere, NH_3
625 exhibits high capability of neutralizing acid gases, thereby slowing down the formation
626 of acid rain and actively participating in the production of sulfates (SO_4^{2-}) and NO_3^- .
627 With the substantial reduction in acidic pollutants, the secondary formation of
628 ammonium sulfate and ammonium nitrate aerosols would decline, leading to an
629 enhanced proportion of gaseous NH_3 in RDN. Given much larger V_d of gaseous NH_3
630 than that of particulate NH_4^+ , the enhanced NH_3 would result in a growth in dry
631 deposition of RDN, thus slowing the decline of total RDN deposition.

632 **3.4 Responses of future Nr deposition to emission perturbation**

633 Figure 67 shows the predicted response of Nr deposition to a 20% emission
634 reduction for 2010s and 2060s under different emission scenarios. The response was
635 obtained by calculating the ratio of the percent change in deposition to that in emissions.
636 For OXN, the nationwide average response of OXN deposition to NO_x emissions was
637 83% for the 2010s (Figure 6a7a). There was a clear north-south difference in the
638 response over EC. We defined Northern China (NC, 30°N-45°N, 110°E-125°E) and

639 Southern China (SC, 20°N-30°N, 110°E-125°E, Figure S1) and calculated the response
640 of OXN deposition to NO_x emission change at 83% and 96%, respectively (Table 5).
641 As a comparison, Liu et al. (2022) reported the response of OXN deposition to NO_x
642 emissions ranging 55-76% in North China Plain and neighboring areas during the 2010s.
643 High ratio of NO_x to VOCs emissions in NC resulted in the NO_x-saturated regime for
644 O₃ formation, and reduced NO_x emissions enhanced the atmospheric oxidation capacity
645 (AOC) and in turn promoted the production of atmospheric ~~nitric acid (HNO₃)~~.
646 Additionally, there was insufficient ambient free NH₃ to completely neutralize the
647 gaseous HNO₃, an important component of OXN_DDEP (Liu et al., 2018; Zhai et al.,
648 2021). The relatively large proportion of HNO₃ in OXN restrained fast decline of
649 OXN_DDEP, given the larger V_d of HNO₃ compared to that of NO₂. Overall, the
650 enhanced AOC, coupled with relatively NH₃-poor condition, resulted in a weak
651 response of OXN deposition to emissions reduction. In our simulations, emissions were
652 controlled for all species including VOCs. Compared to Liu et al. (2022) with NO_x
653 emission reduction only, the extra VOCs emissions reduction might lower AOC due to
654 their great contribution to the formation of O₃ and OH radicals in the atmosphere
655 (McDonald et al., 2018). Thus, the moderately large response in our simulation resulted
656 from the simultaneous reduction of VOC and NO_x emissions, which would partially
657 offset the AOC enhancement induced by NO_x emission control alone, and thereby
658 restrain the OXN deposition to some extent.

659 Similar to the 2010s, the response of OXN deposition to a 20% emission reduction
660 in the 2060s would be 84% over NC under the “Baseline” scenario, in which VOCs and
661 NO_x emissions would remain high levels (Table 5). A 20% reduction in emissions
662 would lead to a 17% decline in near-surface annual mean NO₂ concentrations (Figure
663 S5a in the supplement) but a 3.2% growth in O₃ concentration in NC (Figure S5b). In
664 contrast, under the scenarios of “Current-goal” and “Neutral-goal”, a 20% emission
665 reduction would result in 0.82% and 2.7% decline in near-surface O₃ concentration,
666 respectively (Figure S5b), indicating a weakening non-linear mechanism between
667 emission reduction and AOC enhancement with long-term control of air pollution.

668 Meanwhile, the annual mean HNO_3 concentrations would decrease by 14% and 19%
669 (Figure S5c), and OXN_DDEP would decrease by 18% and 19% (Figure S5d) in
670 “Current-goal” and “Neutral-goal” scenarios, respectively. The reductions would be
671 greater than those for the historical period and the future “Baseline” scenario (10% and
672 11% for HNO_3 concentration and 14% and 14% for OXN_DDEP, respectively).
673 Consequently, the response of total OXN deposition to emission controls would reach
674 92% and 95%, respectively. Compared to NC, greater effectiveness of emission
675 abatement on decreasing OXN deposition was found in SC for both 2010s and all the
676 future scenarios in 2060s. The response was estimated to range 93%-103.00% (Table
677 5), similar to the results of 80-120% in the United States (Tan et al., 2020).

678 The response of RDN deposition to a 20% reduction of emissions was estimated
679 at 96% in 2010s, clearly larger than that in the United States (60-80%, Tan et al., 2020).
680 The value would decline to 94% and 92% for “Current-goal” and “Neutral-goal”
681 scenarios in 2060s, respectively, implying that the national air quality and carbon
682 neutrality policies would enhance the nonlinear response of RDN deposition to
683 precursor emission change, towards current US condition. As mentioned in previously,
684 part of the reason could be the transition to a more NH_3 -rich condition in the future,
685 resulting from more stringent emission controls of SO_2 and NO_x than NH_3 . The
686 proportion of gaseous NH_3 (with larger V_d than particulate NH_4^+) to total RDN would
687 be enhanced, which would in turn delay the reducing RDN deposition. In addition, our
688 simulations did not account for the bidirectional feedback between atmospheric NH_3
689 and soil. Soil volatilization could weaken the sensitivity of dry deposition of RDN to
690 changing NH_3 emissions.

691 **4 Conclusion remarks**

692 Combining two global SSP-RCP climate change pathways and three Chinese
693 emission control scenarios, we assessed the spatiotemporal evolution of future
694 atmospheric Nr deposition in China, its main driving factors, and the changing response
695 of Nr deposition to precursor emission controls. Under the SSP5-8.5 ~~pathway~~, the total

696 Nr deposition would increase from 14.7 in 2010s to 15.4 kg N ha⁻¹ yr⁻¹ in 2060s, and
697 the spatial pattern of deposition would largely be modulated by climate change. In
698 contrast, under the SSP2-4.5 ~~pathway~~, Nr deposition is predicted to decrease to 9.0 kg
699 N ha⁻¹ yr⁻¹ by the 2060s, strongly driven by emissions changes. Implementation of Our
700 predictions of future total Nr deposition were generally lower than those from previous
701 global-scale studies, particularly the results of Galloway et al. (2004). They found that
702 Nr deposition flux in most of East Asia would exceed 50 kg N ha⁻¹ yr⁻¹ by 2050 under
703 the old emission scenario of IPCC92a. The results from ACCMIP datasets that relied
704 on RCPs framework are more comparable to our study. Specifically, Lamarque et al.
705 (2013b) reported that the region-averaged Nr deposition in East Asia would reach 6.9-
706 10.2 kg N ha⁻¹ yr⁻¹ by 2100, which is roughly in line with our results (9.0-15.4 kg N ha⁻
707 1 yr⁻¹) in the 2060s. Such difference arises from the different assumptions on the
708 changing air pollutant emissions in China across studies. By considering China's near-
709 term strict clean air actions and the anticipated long-term emissions controls, the air
710 pollutant emission levels in DPEC (used in this study) are lower than those in any
711 existing CMIP emission scenarios and the earlier IPCC92a scenario (Cheng et al.,
712 2021a). This would result in predictions with lower air pollutant concentrations and
713 deposition. Implementation of stricter clean air and carbon neutrality policies would
714 make RDN become the dominant contributor to future Nr deposition. In the “Neutral-
715 goal” scenario, in particular, the national average OXN deposition was predicted to
716 decrease to 0.98 kg N ha⁻¹ yr⁻¹ by the 2060s, accounting for only 17% of the total Nr
717 deposition. Previous studies at the global scale have also indicated the increasing role
718 of RDN deposition in the future, but the growth of RDN share was commonly predicted
719 to be slower, due to insufficient knowledge on China’s actions on NO_x emission
720 controls. For example, ACCMIP, as reported by Sun et al. (2020), expected that the
721 ratio of RDN to total Nr deposition in eastern China will increase to only 56% by the
722 end of the century.

723 Through experiments with fixed WC emissions, we further revealed that the OXN
724 deposition from WC to EC in the 2060s would increase by 0.30 kg N ha⁻¹ yr⁻¹ (2%)

725 compared to the 2010s under the “Baseline”, but decline by 0.28 kg N ha⁻¹ yr⁻¹ (56%)
726 and 0.51 kg N ha⁻¹ yr⁻¹ (27%) under the “Current-goal” and “Neutral-goal” scenarios,
727 respectively. Similarly, the outflow OXN fluxes from EC in 2060s would decline 94.45
728 kg N s⁻¹ (49%) and 172.86 kg N s⁻¹ (89%) in the latter two scenarios in 2060s,
729 respectively. The response of OXN deposition to a 20% abatement of emissions in NC
730 was estimated at 84% under the “Baseline” scenario, while it would approach 100% in
731 the “Current-goal” and “Neutral-goal” scenarios with the declining share of gaseous
732 HNO₃ in OXN due to weakened AOC. In contrast, the response of RDN deposition to
733 a 20% abatement of emissions would decline in the latter two scenarios, attributed
734 partly to a more NH₃-rich condition and thereby a growing share of gaseous NH₃ in
735 2060s.

736 Our study suggests that future rigorous implementation of clean air and carbon
737 neutrality policies can mitigate the adverse effects of climate change on Nr deposition,
738 and weaken the transport of air pollution to West Pacific. It highlights the potential
739 changes in the source-sink relationship for China, and supports scientific analyses on
740 sources and mitigation of Nr pollution, not only for China but also for downwind areas.
741 More attention needs to be paid to NH₃ emission controls due to its increasing
742 importance on Nr deposition. The sharp decline in future Nr deposition driven by
743 profound emission abatement may substantially reduce the ecological damages like
744 acidification and eutrophication. Meanwhile, it might potentially weaken the carbon
745 sink capacity of terrestrial ecosystems. A comprehensive consideration of the balance
746 between Nr control and terrestrial carbon sinks is essential for the future.

747 Our findings are subject to some limitations. Firstly, given the computationally
748 intensive of numerical simulation, the Nr deposition was simulated with a single model
749 (CMAQ) in this work. As suggested by the MICS-Asia III project, there existed clear
750 difference in Nr deposition simulation among multiple CTMs, and in particular the
751 consistency of dry deposition of OXN was relatively poor, with coefficient of variation
752 (CV) ranging 0.4-0.5 throughout most of China (Ge et al., 2020). Multi-model ensemble
753 methodology is thus recommended in future work to reduce the bias of single-model

754 simulation. Secondly, the role of climate change on future Nr deposition might be
755 underestimated. Climate-driven effects on emissions were not considered in this study,
756 such as the increase of NH₃ volatilization due to global warming (Ren et al., 2023). In
757 addition, we mainly addressed the future evolution of Nr deposition under the mean
758 state of climate, but neglected the potential impact of extreme climatic events. For
759 example, the changing frequency of heavy precipitation was reported as a key factor
760 influencing the variation of Nr deposition (Chen et al., 2023). Therefore, more analyses
761 should be conducted on the connection between the changing extreme climate events
762 and atmospheric deposition.

763 **Data availability**

764 All data in this study are available from the authors upon request.

765 **Author contributions**

766 MMA developed the strategy and methodology of the work and wrote the draft. Y
767 Zhao improved the methodology and revised the manuscript. JCao provided useful
768 comments on the paper. BZheng provided the historical emission inventory. DTong
769 provided the future emission inventory.

770 **Competing interests**

771 The authors declare that they have no conflict of interest.

772 **Acknowledgments**

773 This work was sponsored by National Key Research and Development Program of
774 China (2023YFC3709802) and the National Natural Science Foundation of China
775 (42177080). We are grateful to the High Performance Computing Center (HPCC) of
776 Nanjing University for doing the numerical calculations in this paper on its blade cluster
777 system. We would also like to thank Tsinghua University for the free use of national

778 emissions data (MEIC and DPEC), European Weather Forecasting Center for the free
779 download of meteorological reanalysis data.
780

781 **References**

782 [Alexandrov, G. A., Ginzburg, V. A., Insarov, G. E. & Romanovskaya, A. A. \(2021\).](#)
783 [CMIP6 model projections leave no room for permafrost to persist in Western](#)
784 [Siberia under the SSP5-8.5 scenario. Climatic Change, 169\(3\), 42.](#)
785 <https://doi.org/10.1007/s10584-021-03292-w>

786 Appel, W., Napelenok, S., Hogrefe, C., Pouliot, G., Foley, K., Roselle, S., Pleim, J.,
787 Bash, J., Pye, H., Heath, N., Murphy, B., & Mathur, R. (2017). Overview and
788 Evaluation of the Community Multiscale Air Quality (CMAQ) Modeling System
789 Version 5.2. Chapter 11, Air Pollution Modeling and its Application XXV.
790 Springer International Publishing AG, Cham (ZG), Switzerland, 69-73.
791 https://doi.org/10.1007/978-3-319-57645-9_11

792 [Benish, S. E., Bash, J. O., Foley, K. M., Appel, K. W., Hogrefe, C., Gilliam, R., &](#)
793 [Pouliot, G. \(2022\). Long-term regional trends of nitrogen and sulfur deposition in](#)
794 [the United States from 2002 to 2017. Atmospheric Chemistry and Physics, 22\(19\),](#)
795 [12749–12767. https://doi.org/10.5194/acp-22-12749-2022](#)

796 Bey, I., Jacob, D. J., Yantosca, R. M., Logan, J. A., Field, B. D., Fiore, A. M., Li, Q.,
797 Liu, H. Y., Mickley, L. J., & Schultz, M. G. (2001). Global modeling of
798 tropospheric chemistry with assimilated meteorology: Model description and
799 evaluation. Journal of Geophysical Research: Atmospheres, 106(D19), 23073-
800 23095. <https://doi.org/10.1029/2001JD000807>

801 Carvalho, D., Rocha, A., Gómez-Gesteira, M., & Santos, C. (2012). A sensitivity study
802 of the WRF model in wind simulation for an area of high wind energy.
803 Environmental Modelling & Software, 33, 23–34.
804 <https://doi.org/10.1016/j.envsoft.2012.01.019>

805 Chang, J. S., Brost, R. A., Isaksen, I. S. A., Madronich, S., Middleton, P., Stockwell, W.

806 R., & Walcek, C. J. (1987). A three-dimensional Eulerian acid deposition model:
807 Physical concepts and formulation. *Journal of Geophysical Research:*
808 *Atmospheres*, 92(D12), 14681-14700. <https://doi.org/10.1029/JD092iD12p14681>

809 Chang, M., Cao, J., Ma, M., Liu, Y., Liu, Y., Chen, W., Fan, Q., Liao, W., Jia, S., &
810 Wang, X. (2020). Dry deposition of reactive nitrogen to different ecosystems
811 across eastern China: A comparison of three community models. *Science of The*
812 *Total Environment*, 720, 137548. <https://doi.org/10.1016/j.scitotenv.2020.137548>

813 Chang, Y., Huang, R. J., Ge, X., Huang, X., Hu, J., Duan, Y., Zou, Z., Liu, X., &
814 Lehmann, M. F. (2020). Puzzling haze events in China during the coronavirus
815 (COVID-19) shutdown. *Geophysical Research Letters*, 47(12), e2020GL088533.
816 <https://doi.org/10.1029/2020GL088533>

817 Chen, C., Xiao, W., & Chen, H. Y. (2023). Mapping global soil acidification under N
818 deposition. *Global Change Biology*, 29(16), 4652-4661.
819 <https://doi.org/10.1111/gcb.16813>

820 Chen, Y., Zhang, L., Henze, D. K., Zhao, Y., Lu, X., Winiwarter, W., Guo, Y., Liu, X.,
821 Wen, Z., & Song, Y. (2021). Interannual variation of reactive nitrogen emissions
822 and their impacts on PM_{2.5} air pollution in China during 2005–2015.
823 *Environmental Research Letters*, 16(12), 125004. [https://doi.org/10.1088/1748-](https://doi.org/10.1088/1748-9326/ac3695)
824 [9326/ac3695](https://doi.org/10.1088/1748-9326/ac3695)

825 Cheng, F. Y., Feng, C. Y., Yang, Z. M., Hsu, C. H., Chan, K. W., Lee, C. Y., & Chang,
826 S. C. (2021). Evaluation of real-time PM_{2.5} forecasts with the WRF-CMAQ
827 modeling system and weather-pattern-dependent bias-adjusted PM_{2.5} forecasts in
828 Taiwan. *Atmospheric Environment*, 244, 117909.
829 <https://doi.org/10.1016/j.atmosenv.2020.117909>

830 Cheng, J., Tong, D., Liu, Y., Geng, G., Davis, S. J., He, K., & Zhang, Q. (2023). A
831 synergistic approach to air pollution control and carbon neutrality in China can
832 avoid millions of premature deaths annually by 2060. *One Earth*, 6(8), 978-989.
833 <https://doi.org/10.1016/j.oneear.2023.07.007>

834 Cheng, J., Tong, D., Liu, Y., Yu, S., Yan, L., Zheng, B., Geng, G., He, K., & Zhang, Q.

835 (2021a). Comparison of current and future PM_{2.5} air quality in China under
836 CMIP6 and DPEC emission scenarios. *Geophysical Research Letters*, 48(11),
837 e2021GL093197. <https://doi.org/10.1029/2021GL093197>

838 Cheng, J., Tong, D., Zhang, Q., Liu, Y., Lei, Y., Yan, G., Yan, L., Yu, S., Cui, R. Y.,
839 Clarke, L., Geng, G. N., Zheng, B., Zhang, X. Y., Davis, J. S., & He, K. B. (2021b).
840 Pathways of China's PM_{2.5} air quality 2015–2060 in the context of carbon
841 neutrality. *National Science Review*, 8(12), nwab078.
842 <https://doi.org/10.1093/nsr/nwab078>

843 Chen, W., Jia, S., Wang, X., Shao, M., Liao, W., Guenther, A., Flechard, C., Yu, P.,
844 Zhong, B., Chang, M., Wang, W., Mao, J., Liu, X., Yu, G., & Carmichael, G.
845 (2023). Precipitation trend increases the contribution of dry reduced nitrogen
846 deposition. *npj Climate and Atmospheric Science*, 6(1), 62.
847 <https://doi.org/10.1038/s41612-023-00390-7>

848 Cook, B. I., Mankin, J. S., Marvel, K., Williams, A. P., Smerdon, J. E., & Anchukaitis,
849 K. J. (2020). Twenty - first century drought projections in the CMIP6 forcing
850 scenarios. *Earth's Future*, 8(6), e2019EF001461.
851 <https://doi.org/10.1029/2019EF001461>

852 De Meij, A., & Vinuesa, J. F. (2014). Impact of SRTM and Corine Land Cover data on
853 meteorological parameters using WRF. *Atmospheric Research*, 143, 351-370.
854 <https://doi.org/10.1016/j.atmosres.2014.03.004>

855 Dong, L., Miao, G., & Wen, W. (2021). China's carbon neutrality policy: Objectives,
856 impacts and paths. *East Asian Policy*, 13(01), 5-18.
857 <https://doi.org/10.1142/S1793930521000015>

858 Ellis, R. A., Jacob, D. J., Sulprizio, M. P., Zhang, L., Holmes, C. D., Schichtel, B. A.,
859 Blett, T., Porter, E., Pardo, L. H., & Lynch, J. A. (2013). Present and future
860 nitrogen deposition to national parks in the United States: critical load exceedances.
861 *Atmospheric Chemistry and Physics*, 13(17), 9083–9095.
862 <https://doi.org/10.5194/acp-13-9083-2013>

863 [Fahey, K. M., Carlton, A. G., Pye, H. O. T., Baek, J., Hutzell, W. T., Stanier, C. O.,](#)

864 [Baker, K. R., Appel, K. W., Jaoui, M., & Offenberg, J. H. \(2017\). A framework for](#)
865 [expanding aqueous chemistry in the Community Multiscale Air Quality \(CMAQ\)](#)
866 [model version 5.1. Geoscientific Model Development, 10\(4\), 1587-1605.](#)
867 <https://doi.org/10.5194/gmd-10-1587-2017>

868 Fowler, D., Coyle, M., Skiba, U., Sutton, M. A., Cape, J. N., Reis, S., Sheppard, L. J.,
869 Jenkins, A., Grizzetti, B., Galloway, J. N. Vitousek, P., Leach, A., Bouwman, A.
870 F., Butterbach-Bahl, K., Dentener, F., Stevenson, D., Amann, M., & Voss, M.
871 (2013). The global nitrogen cycle in the twenty-first century. Philosophical
872 Transactions of the Royal Society B: Biological Sciences, 368(1621), 20130164.
873 <https://doi.org/10.1098/rstb.2013.0164>

874 [Galmarini, S., Koffi, B., Solazzo, E., Keating, T., Hogrefe, C., Schulz, M., Benedictow,](#)
875 [A., Griesfeller, J. J., Janssens-Maenhout, G., Carmichael, G., Fu, J., & Dentener,](#)
876 [F. \(2017\). Coordination and harmonization of the multi-scale, multi-model](#)
877 [activities HTAP2, AQMEII3, and MICS-Asia3: simulations, emission inventories,](#)
878 [boundary conditions, and model output formats. Atmospheric Chemistry and](#)
879 [Physics, 17\(2\), 1543-1555. https://doi.org/10.5194/acp-17-1543-2017](#)

880 Gao, Q., Zhang, X., Liu, L., Lu, X., & Wang, Y. (2023). A database of atmospheric
881 inorganic nitrogen deposition fluxes in China from satellite monitoring. Scientific
882 Data, 10(1), 698. <https://doi.org/10.1038/s41597-023-02607-z>

883 Galloway, J. N., Dentener, F. J., Capone, D. G., Boyer, E. W., Howarth, R. W.,
884 Seitzinger, S. P., Asner, G. P., Cleveland, C. C., Green, P. A., Holland, E. A., Karl,
885 D. M., Michaels, A. F., Porter, J. H., Townsend, A. R., & Vöosmarty, C. J. (2004).
886 Nitrogen cycles: past, present, and future. Biogeochemistry, 70, 153-226.
887 <https://doi.org/10.1007/s10533-004-0370-0>

888 [Gu, B., Ge, Y., Ren, Y., Xu, B., Luo, W., Jiang, H, Gu, B., & Chang, J. \(2012\).](#)
889 [Atmospheric reactive nitrogen in China: sources, recent trends, and damage costs.](#)
890 [Environmental science & technology, 46\(17\), 9420-9427.](#)
891 <https://doi.org/10.1021/es301446g>

892 Ge, B., Itahashi, S., Sato, K., Xu, D., Wang, J., Fan, F., Tan, Q., Fu, J. S., Wang, X.,

893 Yamaji, K., Nagashima, T., Li, J., Kajino, M., Liao, H., Zhang, M., Wang, Z., Li,
894 M., Woo, J. H., Kurokawa, J., Pan, Y., Wu, Q., Liu, X., & Wang, Z. (2020). Model
895 Inter-Comparison Study for Asia (MICS-Asia) phase III: multimodel comparison
896 of reactive nitrogen deposition over China. *Atmospheric Chemistry and Physics*,
897 20(17), 10587–10610. <https://doi.org/10.5194/acp-20-10587-2020>

898 Guenther, A., Jiang, X., Heald, C. L., Sakulyanontvittaya, T., Duhl, T., Emmons, L. K.,
899 & Wang, X. (2012). The Model of Emissions of Gases and Aerosols from Nature
900 version 2.1 (MEGAN2.1): an extended and updated framework for modeling
901 biogenic emissions. *Geoscientific Model Development*, 5(6), 1471-1492.
902 <https://doi.org/10.5194/gmd-5-1471-2012>

903 Han, X., Zhang, M., Skorokhod, A., & Kou, X. (2017). Modeling dry deposition of
904 reactive nitrogen in China with RAMS-CMAQ. *Atmospheric Environment*, 166,
905 47-61. <https://doi.org/10.1016/j.atmosenv.2017.07.015>

906 Hertel, O., Skjøth, C. A., Løfstrøm, P., Geels, C., Frohn, L. M., Ellermann, T., &
907 Madsen, P. V. (2006). Modelling Nitrogen Deposition on a Local Scale—A
908 Review of the Current State of the Art. *Environmental Chemistry*, 3(5), 317.
909 <https://doi.org/10.1071/EN06038>

910 Hersbach, H., Bell, B., Berrisford, P., Hirahara, S., Horányi, A., Muñoz-Sabater, J.,
911 Nicolas, J., Peubey, C., Radu, R., Schepers, D., Simmons, A., Soci, C., Abdalla,
912 S., Abellan, X., Balsamo, G., Bechtold, P., Biavati, G., Bidlot, J., Bonavita, M., De
913 Chiara, G., Dahlgren, P., Dee, D., Diamantakis, M., Dragani, R., Flemming, J.,
914 Forbes, R., Fuentes, M., Geer, A., Haimberger, L., Healy, S., Hogan, R. J., Hólm,
915 E., Janisková, M., Keeley, S., Laloyaux, P., Lopez, P., Lupu, C., Radnoti, G., de
916 Rosnay, P., Rozum, I., Vamborg, F., Villaume, S., & Thépaut, J. -N. (2020).
917 *Quarterly Journal of the Royal Meteorological Society*, 146(730), 1999-2049.
918 <https://doi.org/10.1002/qj.3803>

919 Huang, X., Swain, D. L., & Hall, A. D. (2020). Future precipitation increase from very
920 high resolution ensemble downscaling of extreme atmospheric river storms in
921 California. *Science advances*, 6(29), eaba1323.

922 <https://doi.org/10.1126/sciadv.aba1323>

923 IPCC, 2021. Climate Change 2021: The Physical Science Basis. Contribution of
924 Working Group I to the Sixth Assessment Report of the Intergovernmental Panel
925 on Climate Change, Cambridge.

926 Kanakidou, M., Myriokefalitakis, S., Daskalakis, N., Fanourgakis, G., Nenes, A., Baker,
927 A. R., Tsigaridis, K., & Mihalopoulos, N. (2016). Past, Present, and Future
928 Atmospheric Nitrogen Deposition. *Journal of the Atmospheric Sciences*, 73(5),
929 2039–2047. <https://doi.org/10.1175/JAS-D-15-0278.1>

930 Kawase, H., Hara, M., Yoshikane, T., Ishizaki, N. N., Uno, F., Hatsushika, H., & Kimura,
931 F. (2013). Altitude dependency of future snow cover changes over Central Japan
932 evaluated by a regional climate model. *Journal of Geophysical Research:*
933 *Atmospheres*, 118(22), 12-444. <https://doi.org/10.1002/2013JD020429>

934 Kang, Y., Liu, M., Song, Y., Huang, X., Yao, H., Cai, X., Zhang, H., Kang, L., Liu, X.,
935 Yan, X., He, H., Zhang, Q., Shao, M., & Zhu, T. (2016). High-resolution ammonia
936 emissions inventories in China from 1980 to 2012. *Atmospheric Chemistry and*
937 *Physics*, 16(4), 2043–2058. <https://doi.org/10.5194/acp-16-2043-2016>

938 Kim, J. E., Han, Y. J., Kim, P. R., & Holsen, T. M. (2012). Factors influencing
939 atmospheric wet deposition of trace elements in rural Korea. *Atmospheric*
940 *Research*, 116, 185-194. <https://doi.org/10.1016/j.atmosres.2012.04.013>

941 Koetse, M. J., & Rietveld, P. (2009). The impact of climate change and weather on
942 transport: An overview of empirical findings. *Transportation Research Part D:*
943 *Transport and Environment*, 14(3), 205-221.
944 <https://doi.org/10.1016/j.trd.2008.12.004>

945 Lamarque, J. -F., Dentener, F., McConnell, J., Ro, C. -U., Shaw, M., Vet, R., Bergmann,
946 D., Cameron-Smith, P., Dalsoren, S., Doherty, R., Faluvegi, G., Ghan, S. J., Josse,
947 B., Lee, Y. H., MacKenzie, I. A., Plummer, D., Shindell, D. T., Skeie, R. B.,
948 Stevenson, D. S., Strode, S., Zeng, G., Curran, M., Dahl-Jensen, D., Das, S.,
949 Fritzsche, D., & Nolan, M. (2013a,2013b). Multi-model mean nitrogen and sulfur
950 deposition from the Atmospheric Chemistry and Climate Model Intercomparison

951 Project (ACCMIP): evaluation of historical and projected future changes.
952 Atmospheric Chemistry and Physics, 13(16), 7997–8018.
953 <https://doi.org/10.5194/acp-13-7997-2013>

954 Lamarque, J.-F., Shindell, D. T., Josse, B., Young, P. J., Cionni, I., Eyring, V.,
955 Bergmann, D., Cameron-Smith, P., Collins, W. J., Doherty, R., Dalsoren, S.,
956 Faluvegi, G., Folberth, G., Ghan, S. J., Horowitz, L. W., Lee, Y. H., MacKenzie,
957 I. A., Nagashima, T., Naik, V., Plummer, D., Righi, M., Rumbold, S. T., Schulz,
958 M., Skeie, R. B., Stevenson, D. S., Strode, S., Sudo, K., Szopa, S., Voulgarakis,
959 A., & Zeng, G. (~~2013b~~2013a). The Atmospheric Chemistry and Climate Model
960 Intercomparison Project (ACCMIP): overview and description of models,
961 simulations and climate diagnostics. Geoscientific Model Development, 6(1),
962 179–206. <https://doi.org/10.5194/gmd-6-179-2013>

963 Lauer, A., Zhang, C., Elison-Timm, O., Wang, Y., & Hamilton, K. (2013). Downscaling
964 of climate change in the Hawaii region using CMIP5 results: On the choice of the
965 forcing fields. Journal of Climate, 26(24), 10006-10030.
966 <https://doi.org/10.1175/JCLI-D-13-00126.1>

967 Li, M., Liu, H., Geng, G., Hong, C., Liu, F., Song, Y., Tong, D., Zheng, B., Cui, H.,
968 Man, H., Zhang, Q., & He, K. (2017). Anthropogenic emission inventories in
969 China: a review. National Science Review, 4(6), 834-866.
970 <https://doi.org/10.1093/nsr/nwx150>

971 Li, M., Zhang, Q., Kurokawa, J. -I., Woo, J. -H., He, K., Lu, Z., Ohara, T., Song, Y.,
972 Streets, D. G., Carmichael, G. R., Cheng, Y., Hong, C., Huo, H., Jiang, X., Kang,
973 S., Liu, F., Su, H., and Zheng, B. (2017). MIX: a mosaic Asian anthropogenic
974 emission inventory under the international collaboration framework of the MICS-
975 Asia and HTAP. Atmospheric Chemistry and Physics, 17(2), 935-963.
976 <https://doi.org/10.5194/acp-17-935-2017>

977 Liao, J., Wang, T., Jiang, Z., Zhuang, B., Xie, M., Yin, C., Wang, X., Zhu, J., Fu, Y.,
978 & Zhang, Y (2015). WRF/Chem modeling of the impacts of urban expansion on
979 regional climate and air pollutants in Yangtze River Delta, China. Atmospheric

980 Environment, 106, 204-214. <https://doi.org/10.1016/j.atmosenv.2015.01.059>

981 Liu, L., [Wen, Z., Liu, S., Zhang, X., & Liu, X. \(2024\). Decline in atmospheric nitrogen](#)
982 [deposition in China between 2010 and 2020. Nature Geoscience, 17\(8\), 733-736.](#)
983 <https://doi.org/10.1038/s41561-024-01484-4>

984 [Liu, L.,](#) Zhang, X., Xu, W., Liu, X., Zhang, Y., Li, Y., Wei, J., Lu, X., Wang, S., Zhang,
985 W., Zhao, L., Wang, Z., & Wu, X. (2020). Fall of oxidized while rise of reduced
986 reactive nitrogen deposition in China. Journal of Cleaner Production, 272, 122875.
987 <https://doi.org/10.1016/j.jclepro.2020.122875>

988 Liu, M., Huang, X., Song, Y., Xu, T., Wang, S., Wu, Z., Hu, M., Zhang, L., Zhang, Q.,
989 Pan, Y., Liu, X., & Zhu, T. (2018). Rapid SO₂ emission reductions significantly
990 increase tropospheric ammonia concentrations over the North China Plain.
991 Atmospheric Chemistry and Physics, 18, 17933-17943.
992 <https://doi.org/10.5194/acp-18-17933-2018>

993 Liu, M., Shang, F., Lu, X., Huang, X., Song, Y., Liu, B., Zhang, Q., Liu X., Cao, J., Xu,
994 T., Wang T., Xu, Z., Xu, W., Liao W., Kang L., Cai, X., Zhang, H, Dai, Y., & Liu,
995 X. (2022). Unexpected response of nitrogen deposition to nitrogen oxide controls
996 and implications for land carbon sink. Nature Communications, 13(1), 3126.
997 <https://doi.org/10.1038/s41467-022-30854-y>

998 Liu, S., Xing, J., Wang, S., Ding, D., Cui, Y., & Hao, J. (2021). Health benefits of
999 emission reduction under 1.5° C pathways far outweigh climate-related variations
1000 in China. Environmental Science & Technology, 55(16), 10957-10966.
1001 <https://doi.org/10.1021/acs.est.1c01583>

1002 [Liu, X., & Du, E. \(2020\). An overview of atmospheric reactive nitrogen in China from](#)
1003 [a global perspective. Atmospheric Reactive Nitrogen in China: Emission,](#)
1004 [Deposition and Environmental Impacts, 1-10. https://doi.org/10.1007/978-981-](#)
1005 [13-8514-8_1](#)

1006 Liu X., Xu W., Duan, L., Du, E., Pan, Y., Lu, X., Zhang, L., Wu, Z., Wang, X., Zhang,
1007 Y., Shen, J., Song, L., Feng, Z., Liu, X., Song, W., Tang, A., Zhang, Y., Zhang, X
1008 & Collett, J. L. (2017). Atmospheric nitrogen emission, deposition, and air quality

1009 impacts in China: an overview. *Current Pollution Reports*, 3, 65-77.
1010 <https://doi.org/10.1007/s40726-017-0053-9>

1011 Liu, X., Zhang, Y., Han, W., Tang, A., Shen, J., Cui, Z., Vitousek, P., Erisman, J. W.,
1012 Goulding, K., Christie, P., Fangmeier, A., & Zhang, F. (2013). Enhanced nitrogen
1013 deposition over China. *Nature*, 494(7438), 459–462.
1014 <https://doi.org/10.1038/nature11917>

1015 Liu, X. H., Zhang, Y., Cheng, S. H., Xing, J., Zhang, Q., Streets, D. G., Yang, C., Wang,
1016 W. X., & Hao, J. M. (2010). Understanding of regional air pollution over China
1017 using CMAQ, part I performance evaluation and seasonal variation. *Atmospheric*
1018 *Environment*, 44(20), 2415-2426. <https://doi.org/10.1016/j.atmosenv.2010.03.035>

1019 Liu Y., & Wang T. (2020). Worsening urban ozone pollution in China from 2013 to
1020 2017—Part 1: The complex and varying roles of meteorology. *Atmospheric*
1021 *Chemistry and Physics*, 20(11), 6305-6321. [https://doi.org/10.5194/acp-20-6305-](https://doi.org/10.5194/acp-20-6305-2020)
1022 [2020](https://doi.org/10.5194/acp-20-6305-2020)

1023 Ma, M., Zheng, B., Xu, W., Cao, J., Zhou, K., & Zhao, Y. (2023). Trend and Interannual
1024 Variations of Reactive Nitrogen Deposition in China During 2008–2017 and the
1025 Roles of Anthropogenic Emissions and Meteorological Conditions. *Journal of*
1026 *Geophysical Research: Atmospheres*, 128(6), e2022JD037489.
1027 <https://doi.org/10.1029/2022JD037489>

1028 McDonald, B., De Gouw, J., Gilman, J., Jathar, S., Akherati, A., Cappa, C., Jinenez, J.,
1029 Le-Taylor, J., Hayes, P., Mckeen, S., Cui, Y., Kim, S., Gentner, D., Isaacman-
1030 Vanwertz, G., Goldstein, A., Harley, R., Frost, G., Roberts, J., Ryerson, T., &
1031 Trainer, M. (2018). Volatile chemical products emerging as largest petrochemical
1032 source of urban organic emissions. *Science*, 359(6377), 760-764.
1033 <https://doi.org/10.1126/science.aag0524>

1034 [Meinshausen, M., Nicholls, Z. R. J., Lewis, J., Gidden, M. J., Vogel, E., Freund, M.,](#)
1035 [Beyerle, U., Gessner, C., Nauels, A., Bauer, N., Canadell, J. G., Daniel, J. S., John,](#)
1036 [A., Krummel, P. B., Luderer, G., Meinshausen, N., Montzka, S. A., Rayner, P. J.,](#)
1037 [Reimann, S., Smith, S. J., van den Berg, M., Velders, G. J. M., Vollmer, M. K., &](#)

1038 [Wang, R. H. J. \(2020\). The shared socio-economic pathway \(SSP\) greenhouse gas](#)
1039 [concentrations and their extensions to 2500. Geoscientific Model Development,](#)
1040 [13\(8\), 3571-3605. https://doi.org/10.5194/gmd-13-3571-2020](#)

1041 Murphy, B. N., Woody, M. C., Jimenez, J. L., Carlton, A. M. G., Hayes, P. L., Liu, S.,
1042 Ng, N. L., Russell, L. M., Setyan, A., Xu, L., Young, J., Zaveri, R. A., Zhang, Q.,
1043 & Pye, H. O. T. (2017). Semivolatile POA and parameterized total combustion
1044 SOA in CMAQv5.2: impacts on source strength and partitioning, Atmospheric
1045 Chemistry and Physics, 17(18), 11107-11133. [https://doi.org/10.5194/acp-2017-](https://doi.org/10.5194/acp-2017-11107-2017)
1046 [11107-2017](https://doi.org/10.5194/acp-2017-11107-2017)

1047 [O'Neill, B. C., Carter, T. R., Ebi, K., Harrison, P. A., Kemp-Benedict, E., Kok, K.,](#)
1048 [Kriegler, E., Preston, B. L., Riahi, K., Sillmann, J., van Ruijven, B. J., van Vuuren,](#)
1049 [D., Carlisle, D., Conde, C., Fuglestvedt, J., Green, C., Hasegawa, T., Leininger, J.,](#)
1050 [Monteith, S., & Pichs-Madruga, R. \(2020\). Achievements and needs for the](#)
1051 [climate change scenario framework. Nature Climate Change, 10\(12\), 1074-1084.](#)
1052 <https://doi.org/10.1038/s41558-020-00952-0>

1053 O'Neill, B. C., Tebaldi, C., Van Vuuren, D. P., Eyring, V., Friedlingstein, P., Hurtt, G.,
1054 Knutti, R., Kriegler, E., Lamarque, J. -F., Lowe, J., Meehl, G. A., Moss, R., Riahi,
1055 K & Sanderson, B. M. (2016). The scenario model intercomparison project
1056 (ScenarioMIP) for CMIP6. Geoscientific Model Development, 9(9), 3461-3482.
1057 <https://doi.org/10.5194/gmd-9-3461-2016>

1058 Pineda, N., Jorba, O., Jorge, J., & Baldasano, J. M. (2004). Using NOAA AVHRR and
1059 SPOT VGT data to estimate surface parameters: application to a mesoscale
1060 meteorological model. International journal of remote sensing, 25(1), 129-143.
1061 <https://doi.org/10.1080/0143116031000115201>

1062 Pye, H. O. T., Murphy, B. N., Xu, L., Ng, N. L., Carlton, A. G., Guo, H., Weber, R.,
1063 Vasilakos, P., Appel, K. W., Budisulistiorini, S. H., Surratt, J. D., Nenes, A., Hu,
1064 W., Jimenez, J. L., Isaacman-VanWertz, G., Misztal, P. K., & Goldstein, A. H.
1065 (2017). On the implications of aerosol liquid water and phase separation for
1066 organic aerosol mass. Atmospheric Chemistry and Physics, 17(1), 343-369.

1067 <https://doi.org/10.5194/acp-17-343-2017>

1068 Raza, S, Miao, N, Wang, P, Ju, X., Chen, Z., Zhou, J., & Kuzyakov Y. (2020). Dramatic
1069 loss of inorganic carbon by nitrogen - induced soil acidification in Chinese
1070 croplands. *Global change biology*, 26(6), 3738-3751.
1071 <https://doi.org/10.1111/gcb.15101>

1072 Sahu, S. K., Gelfand, A. E., & Holland, D. M. (2010). Fusing point and areal level
1073 space-time data with application to wet deposition. *Journal of the Royal Statistical*
1074 *Society Series C: Applied Statistics*, 59(1), 77-103. [https://doi.org/10.1111/j.1467-](https://doi.org/10.1111/j.1467-9876.2009.00685.x)
1075 [9876.2009.00685.x](https://doi.org/10.1111/j.1467-9876.2009.00685.x)

1076 Sarwar, G., Luecken, D.J., Yarwood, G., Whitten, G.D., & Carter, W.P. (2008). Impact
1077 of an updated carbon bond mechanism on predictions from the CMAQ modeling
1078 system: preliminary assessment. *Journal of Applied Meteorology and Climatology*,
1079 47(1), 3-14. <https://doi.org/10.1175/2007JAMC1393.1>

1080 Shen, A., Liu, Y., Lu, X., Xu, Y., Jin, Y., Wang, H., Zhang, J., Wang, X., Chang, M.,
1081 & Fan, Q (2023). Modeling regional nitrogen cycle in the atmosphere: Present
1082 situation and its response to the future emissions control strategy. *Science of The*
1083 *Total Environment*, 891, 164379. <https://doi.org/10.1016/j.scitotenv.2023.164379>

1084 Shen, Y., Jiang, F., Feng, S., Zheng, Y., Cai, Z., & Lyu, X. (2021). Impact of weather
1085 and emission changes on NO₂ concentrations in China during 2014–2019.
1086 *Environmental Pollution*, 269(15), 116163.
1087 <https://doi.org/10.1016/j.envpol.2020.116163>

1088 Shi, X., Zheng, Y., Lei, Y., Xue, W., Yan, G., Liu, X., Cai, B., Tong, D., & Wang, J.
1089 (2021). Air quality benefits of achieving carbon neutrality in China. *Science of the*
1090 *Total Environment*, 795, 148784. <https://doi.org/10.1016/j.scitotenv.2021.148784>

1091 Skamarock W C & Klemp J B. (2008). A time-split nonhydrostatic atmospheric model
1092 for weather research and forecasting applications. *Journal of Computational*
1093 *Physics*, 227(7), 3465-3485. <https://doi.org/10.1016/j.jcp.2007.01.037>

1094 Skamarock, W. C., Klemp, J. B., Dudhia, J., Gill, D. O., Barker, D., Duda, M. G., Huang,

1095 X.-Y., Wang, W., & Powers, J. G. (2008). A Description of the Advanced Research
1096 WRF Version 3, NCAR technical note, NCAR/TN-475+STR.
1097 <https://doi.org/10.5065/D68S4MVH>

1098 Su, B., Huang, J., Mondal, S. K., Zhai, J., Wang, Y., Wen, S., Gao, M., Lv, Y., Jiang, S.,
1099 Jiang, T., & Li, A. (2021). Insight from CMIP6 SSP-RCP scenarios for future
1100 drought characteristics in China. Atmospheric Research, 250, 105375.
1101 <https://doi.org/10.1016/j.atmosres.2020.105375>

1102 Sun, K., Gao, Y., Guo, X., Zhang, J., Zeng, X., Ma, M., Chen, Y., Luo, K., Yao, X., &
1103 Gao, H. (2022). The enhanced role of atmospheric reduced nitrogen deposition in
1104 future over East Asia–Northwest Pacific. *Science of The Total Environment*, 833,
1105 155146. <https://doi.org/10.1016/j.scitotenv.2022.155146>

1106 Tan, J., Fu, J. S., & Seinfeld, J. H. (2020). Ammonia emission abatement does not fully
1107 control reduced forms of nitrogen deposition. *Proceedings of the National*
1108 *Academy of Sciences*, 117(18), 9771–9775.
1109 <https://doi.org/10.1073/pnas.1920068117>

1110 Taniguchi, K., & Tajima, Y. (2020). Variations in extreme wave events near a South
1111 Pacific Island under global warming: case study of Tropical Cyclone Tomas.
1112 *Progress in Earth and Planetary Science*, 7(1), 1-16.
1113 <https://doi.org/10.1186/s40645-020-0321-y>

1114 Tong, D., Cheng, J., Liu, Y., Yu, S., Yan, L., Hong, C., Qin, Y., Zhao, H., Zheng, Y.,
1115 Geng, G., Li, M., Liu, F., Zhang, Y., Zheng, B., Clarke, L., & Zhang, Q. (2020).
1116 Dynamic projection of anthropogenic emissions in China: methodology and 2015–
1117 2050 emission pathways under a range of socio-economic, climate policy, and
1118 pollution control scenarios, *Atmospheric Chemistry and Physics*, 20(9), 5729–
1119 5757. <https://doi.org/10.5194/acp-20-5729-2020, 2020>

1120 Toyota, K., Dastoor, A. P., & Ryzhkov, A. (2017). Parameterization of gaseous dry
1121 deposition in atmospheric chemistry models: Sensitivity to aerodynamic resistance
1122 formulations under statically stable conditions. Atmospheric Environment, 147,
1123 409-422. <https://doi.org/10.1016/j.atmosenv.2016.09.055>

1124 ~~Wang, X., Tolksdorf, V., Otto, M., & Scherer, D. (2021). WRF based dynamical~~
1125 ~~downscaling of ERA5 reanalysis data for High Mountain Asia: Towards a new~~
1126 ~~version of the High Asia Refined analysis. International Journal of Climatology,~~
1127 ~~41(1), 743-762. <https://doi.org/10.1002/joc.6686>~~

1128 Ummerhofer, C. C., & Meehl, G. A. (2017). Extreme weather and climate events with
1129 ecological relevance: a review. Philosophical Transactions of the Royal Society B:
1130 Biological Sciences, 372(1723), 20160135.
1131 <https://doi.org/10.1098/rstb.2016.0135>

1132 Van Vuuren, D. P., Edmonds, J., Kainuma, M., Riahi, K., Thomson, A., Hibbard, K.,
1133 Hurtt, G. C., Kram, T., Krey, V., Lamarque, J. F., Masui, T., Meinshausen, M.,
1134 Nakicenovic, N., Smith, S. J., & Rose, S. K. (2011). The representative
1135 concentration pathways: an overview. Climatic Change, 109, 5-31.
1136 <https://doi.org/10.1007/s10584-011-0148-z>

1137 Vet, R., Artz, R. S., Carou, S., Shaw, M., Ro, C.-U., Aas, W., Baker, A., Bowersox, V.
1138 C., Dentener, F., Galy-Lacaux, C., Hou, A., Pienaar, J. J., Gillett, R., Forti, M. C.,
1139 Gromov, S., Hara, H., Khodzher, T., Mahowald, N. M., Nickovic, S., Rao, P. S.
1140 P., & Reid, N. W. (2014). A global assessment of precipitation chemistry and
1141 deposition of sulfur, nitrogen, sea salt, base cations, organic acids, acidity and pH,
1142 and phosphorus. Atmospheric Environment, 93, 3-100.
1143 <https://doi.org/10.1016/j.atmosenv.2013.10.060>

1144 Venkatram, A., & Pleim, J. (1999). The electrical analogy does not apply to modeling
1145 dry deposition of particles. Atmospheric Environment, 33(18), 3075-3076.
1146 [https://doi.org/10.1016/S1352-2310\(99\)00094-1](https://doi.org/10.1016/S1352-2310(99)00094-1)

1147 Wang, X., Tolksdorf, V., Otto, M., & Scherer, D. (2021). WRF -based dynamical
1148 downscaling of ERA5 reanalysis data for High Mountain Asia: Towards a new
1149 version of the High Asia Refined analysis. International Journal of Climatology,
1150 41(1), 743-762. <https://doi.org/10.1002/joc.6686>

1151 Wen, Z., Ma, X., Xu, W., Si, R., Liu, L., Ma, M., Zhao, Y., Tang, A., Zhang, Y., Wang,
1152 K., Zhang, Y., Shen, J., Zhang, L., Zhao, Y., Zhang, F., Goulding, K., & Liu, X.

1153 [\(2024\). Combined short-term and long-term emission controls improve air quality](#)
1154 [sustainably in China. Nature Communications, 15\(1\), 5169.](#)
1155 <https://doi.org/10.1038/s41467-024-49539-9>

1156 Wen, Z., Xu, W., Li, Q., Han, M., Tang, A., Zhang, Y., Luo, X., Shen, J., Wang, W.,
1157 Li, K., Pan, Y., Zhang, L., Li, W., Collett Jr, J. L., Zhong, B., Wang, X., Goulding,
1158 K., Zhang, F., & Liu, X. (2020). Changes of nitrogen deposition in China from
1159 1980 to 2018. *Environment International*, 144, 106022.
1160 <https://doi.org/10.1016/j.envint.2020.106022>

1161 Wesely, M. L. (2007). Parameterization of surface resistances to gaseous dry deposition
1162 in regional-scale numerical models. *Atmospheric Environment*, 41, 52-63.
1163 <https://doi.org/10.1016/j.atmosenv.2007.10.058>

1164 ~~Wu, <https://doi.org/10.1021/acs.est.6b03634>~~ Wu, Z., Schwede, D. B., Vet, R., Walkr, J.
1165 T., Shaw, Mike., Staebler, R., & Zhang, L. (2018). Evaluation and Intercomparison
1166 of Five North American Dry Deposition Algorithms at a Mixed Forest Site. *Journal*
1167 *of Advances in Modeling Earth Systems*, 10(7), 1571-1586.
1168 <https://doi.org/10.1029/2017MS001231>~~<https://doi.org/10.1029/2017MS001231>~~

1169 [Xia, W., Wang, Y., Zhang, G. J., & Wang, B. \(2024\). Light Precipitation rather than](#)
1170 [Total Precipitation Determines Aerosol Wet Removal. Environmental Science &](#)
1171 [Technology, in press. <https://doi.org/10.1021/acs.est.4c07684>](#)

1172 Xin, X., Wu, T., Zhang, J., Yao, J., & Fang, Y. (2020). Comparison of CMIP6 and
1173 CMIP5 simulations of precipitation in China and the East Asian summer monsoon.
1174 *International Journal of Climatology*, 40(15), 6423-6440.
1175 <https://doi.org/10.1002/joc.6590>

1176 Xu, W., Liu, L., Cheng, M., Zhao, Y., Zhang, L., Pan, Y., Zhang, X., Gu, B., Li, Y.,
1177 Zhang, X., Shen, J., Lu, L., Luo, X., Zhao, Y., Feng, Z., Collett Jr, J. L., Zhang,
1178 F., & Liu, X. (2018). Spatial-temporal patterns of inorganic nitrogen air
1179 concentrations and deposition in eastern China. *Atmospheric Chemistry and*
1180 *Physics*, 18(5), 10931–10954. <https://doi.org/10.5194/acp-18-10931-2018>

1181 Xu, W., Luo, X., Pan, Y., Zhang, L., Tang, A., Shen . J., Zhang, Y., Li, H., Wu, Q.,

1182 Yang, D., Zhang, Y., Xue, J., Li, W., Li, Q., Tang, L., Lu, S., Liang, T., Tong, Y.,
1183 Liu, P., Zhang, Q., Xiong, Z., Shi, X., Wu, L., Shi, W., Tian, K., Zhong, X., Shi,
1184 K., Tang, Q., Zhang, L., Huang, J., He, C., Kuang, F., Zhu, B., Liu, H., Jin, X.,
1185 Xin, Y., Shi, X., Du, E., Dore, A., Tang, S., Collett Jr, J., Goulding, K., Sun, Y.,
1186 Ren, J., Zhang, F., & Liu, X. (2015) Quantifying atmospheric nitrogen deposition
1187 through a nationwide monitoring network across China. *Atmospheric Chemistry*
1188 *and Physics*, 15(21), 12345–12360. <https://doi.org/10.5194/acp-15-12345-2015>

1189 Xu, W., Zhang, L., & Liu, X. (2019). A database of atmospheric nitrogen concentration
1190 and deposition from the nationwide monitoring network in China. *Scientific Data*,
1191 6(1), 51. <https://doi.org/10.1038/s41597-019-0061-2>

1192 Xu, Z., Han, Y., Tam, C. Y., Yang, Z. L., & Fu, C. (2021). Bias-corrected CMIP6 global
1193 dataset for dynamical downscaling of the historical and future climate (1979–
1194 2100). *Scientific Data*, 8(1), 293. <https://doi.org/10.1038/s41597-021-01079-3>

1195 Yu, G., Jia, Y., He, N., Zhu, J., Chen, Z., Wang, Q., Piao, S., Liu, X., He, H., Guo, X.,
1196 Wen, Z., Li, P., Ding, G., & Goulding, K. (2019). Stabilization of atmospheric
1197 nitrogen deposition in China over the past decade. *Nature Geoscience*, 12(6), 424–
1198 429. <https://doi.org/10.1038/s41561-019-0352-4>

1199 Zhai, S., Jacob, D. J., Wang, X., Liu, Z., Wen, T., Shah, V., Li, K., Moch, J. M., Bates,
1200 K. H., Song, S., Shen, L., Zhang, Y., Luo, G., Yu, F., Sun, Y., Wang, L., Qi, M.,
1201 Tao, J., Gui, K., Xu, H., Zhang, Q., Zhao, T., Wang, Y., Lee, H. C., Choi, H., &
1202 Liao, H. (2021). Control of particulate nitrate air pollution in China. *Nature*
1203 *Geoscience*, 14, 389-395. <https://doi.org/10.1038/s41561-021-00726-z>

1204 Zhang, J., Gao, Y., Leung, L. R., Luo, K., Liu, H., Lamarque, J. -F., Fan J., Yao, X.,
1205 Gao, H., & Nagashima, T. (2019). Impacts of climate change and emissions on
1206 atmospheric oxidized nitrogen deposition over East Asia. *Atmospheric Chemistry*
1207 *and Physics*, 19(2), 887-900. <https://doi.org/10.5194/acp-19-887-2019>

1208 Zhang, L., Chen, Y., Zhao, Y., Henze, D. K., Zhu, L., Song, Y., Paulot, F., Liu, X., Pan,
1209 Y., Lin, Y., & Huang, B. (2018). Agricultural ammonia emissions in China:
1210 reconciling bottom-up and top-down estimates. *Atmospheric Chemistry and*

1211 Physics, 18(1), 339–355. <https://doi.org/10.5194/acp-18-339-2018>

1212 Zhang, Y., Foley, K. M., Schwede, D. B., Bash, J. O., Pinto, J. P., & Dennis, R. L. (2019).
1213 A Measurement-Model Fusion Approach for Improved Wet Deposition Maps and
1214 Trends. *Journal of Geophysical Research: Atmospheres*, 124(7), 4237-4251.
1215 <https://doi.org/10.1029/2018JD029051>

1216 Zhao, B., Wang, S. X., Liu, H., Xu, J. Y., Fu, K., Klimont, Z., Hao, J. M., He, K. B.,
1217 Cofala, J., & Amann, M. (2013). NO_x emissions in China: historical trends and
1218 future perspectives. *Atmospheric Chemistry and Physics*, 13(19), 9869–9897.
1219 <https://doi.org/10.5194/acp-13-9869-2013>

1220 Zhao, Y., Xi, M., Zhang, Q., Dong, Z., Ma, M., Zhou, K., Xu, W., Xing, J., Zheng, B.,
1221 Wen, Z., Liu, X., Nielsen, C. P., Liu, Y., Pan, Y., & Zhang, L. (2022). Decline in
1222 bulk deposition of air pollutants in China lags behind reductions in emissions.
1223 *Nature Geoscience*, 15(3), 190–195. <https://doi.org/10.1038/s41561-022-00899-1>

1224 Zhao, Y., Zhang, L., Chen, Y., Liu, X., Xu, W., Pan, Y., & Duan, L. (2017).
1225 Atmospheric nitrogen deposition to China: A model analysis on nitrogen budget
1226 and critical load exceedance. *Atmospheric Environment*, 153, 32–40.
1227 <https://doi.org/10.1016/j.atmosenv.2017.01.018>

1228 Zheng, B., Tong, D., Li, M., Liu, F., Hong, C., Geng, G., Li, H., Li, X., Peng, L., Qi, J.,
1229 Yan, L., Zhang, Y., Zhao, H., Zheng, Y., He, K., & Zhang, Q. (2018). Trends in
1230 China's anthropogenic emissions since 2010 as the consequence of clean air
1231 actions. *Atmospheric Chemistry and Physics*, 18(19), 14095–14111.
1232 <https://doi.org/10.5194/acp-18-14095-2018>

1233 Zheng, L., Zhai, W., Wang, L., & Huang, T. (2020). Improving the understanding of
1234 central Bohai Sea eutrophication based on wintertime dissolved inorganic nutrient
1235 budgets: Roles of north Yellow Sea water intrusion and atmospheric nitrogen
1236 deposition. *Environmental Pollution*, 267, 115626.
1237 <https://doi.org/10.1016/j.envpol.2020.115626>

1238 Zhou, K., Xu, W., Zhang, L., Ma, M., Liu, X., & Zhao, Y. (2023). Estimating nitrogen
1239 and sulfur deposition across China during 2005 to 2020 based on multiple

1240 statistical models. *Atmospheric Chemistry and Physics*, 23(15), 8531-8551.
1241 <https://doi.org/10.5194/acp-23-8531-2023>

1242 Zhu, H., Chen, Y., Zhao, Y., Zhang, L., Zhang, X., Zheng, B., Liu, L., Pan Y., Xu, W.,
1243 & Liu, X. (2022). The Response of Nitrogen Deposition in China to Recent and
1244 Future Changes in Anthropogenic Emissions. *Journal of Geophysical Research:*
1245 *Atmospheres*, 127(23), e2022JD037437. <https://doi.org/10.1029/2022JD037437>

1246 Zhu, J., Chen, Z., Wang, Q., Xu, L., He, N., Jia, Y., Zhang, Q & Yu, G. (2020). Potential
1247 transition in the effects of atmospheric nitrogen deposition in China.
1248 *Environmental Pollution*, 258, 113739.
1249 <https://doi.org/10.1016/j.envpol.2019.113739>

1250 Zhu, J., Tai, A P K., & Hung Lam Yim, S. (2022). Effects of ozone–vegetation
1251 interactions on meteorology and air quality in China using a two-way coupled
1252 land–atmosphere model. *Atmospheric Chemistry and Physics*, 22(2), 765-782.
1253 <https://doi.org/10.5194/acp-22-765-2022>
1254

1255 **Figure captions**

1256 Figure 1 Evaluations of simulated monthly average temperature at the height of 2 m
1257 (T2, a), wind speed at the height of 10 m (WS10, b), relative humidity (RH, c), and
1258 accumulated precipitation (PREC, d) in Mainland China. The dots represent the site-
1259 level observations. The normalized mean bias (NMB), normalized mean error (NME),
1260 root mean squared error (RMSE) and the correlation coefficient (R) for the comparisons
1261 are shown in the lower left corner of each panel.

1262 Figure 2 Spatial distribution of relative changes (%) of NO_x (a-c) and NH₃
1263 emissions (d-f) from 2010s (2010-2014) to 2060s (2060-2064) for emission scenarios
1264 of “Baseline”, “Current-goal” and “Neutral-goal”. Relative changes are calculated by
1265 comparing 2060s emission levels to 2010s emission levels, then dividing the difference
1266 by the 2010s emission levels.

1267 Figure 3 Spatial distribution of annual averaged Nr deposition fluxes (kg N ha⁻¹ yr⁻¹)
1268 for different forms and species in 2010s and the changes between 2010s and 2060s.
1269 Panels (a-d) represent the results of 2010s (Base simulation case). Panels (e-h) represent
1270 future deposition changes under the SSP2-4.5 pathway (Case 1 – Base case). Panels (i-
1271 l) represent the changes under the SSP5-8.5 pathway (Case 2 – Base case).

1272 Figure 34 Changes in annual total Nr deposition fluxes (kg N ha⁻¹ yr⁻¹) from 2010s to
1273 2060s attributed to climate change (a, d), emission change (b, e), and both (c, f). Panels
1274 (a-c) represent the changes under the SSP2-4.5 pathway, respectively and Panels (d-f)
1275 represent the changes under the SSP5-8.5 pathway. Domain-averaged spatial
1276 correlation (R) between the impact of climate or emission change and both is presented
1277 in panels (a, d) or (b, e).

1278 Figure 45 Changes in OXN (a-c) and RDN deposition (d-f) from 2010s to 2060s
1279 attributed to emission variation in “Baseline”, “Current-goal” and “Neutral-goal”
1280 scenarios.

1281 Figure 56 Relative changes in Nr emissions and deposition as well as the ratio of

1282 changes in OXN outflow to changes in NO_x emissions ($\Delta T/\Delta E$) in WC and EC from
1283 2010s to 2060s under different emission scenarios.

1284 Figure 67 Predicted response (%) of OXN (a-d) and RDN deposition (e-h) to a 20%
1285 perturbation of emissions in 2010s and 2060s for different emission scenarios. The
1286 response is obtained by calculating the ratio of the percent change in deposition to that
1287 in emission.

1288 **Tables**

1289 **Table 1 Description of the designed simulation cases.**

<u>Name</u> <u>Simulations</u>	Emissions input	Meteorological input
Base <u>case</u>	MEIC, 2010-2014	ERA5 reanalysis, 2010-2014
Case1	DPEC “Current-goal”, 2060	SSP2-4.5 BCMM, 2060-2064
Case2	DPEC “Baseline”, 2060	SSP5-8.5 BCMM, 2060-2064
Case3	MEIC, 2010-2014	SSP2-4.5 BCMM, 2060-2064
Case4	MEIC, 2010-2014	SSP5-8.5 BCMM, 2060-2064
Case5	DPEC “Neutral-goal”, 2060	SSP2-4.5 BCMM, 2060-2064
Case6	Same as Case1, but emissions in WC are maintained at 2010s levels.	SSP2-4.5 BCMM, 2060-2064
Case7	Same as Case2, but emissions in WC are maintained at 2010s levels.	SSP5-8.5 BCMM, 2060-2064
Case8	Same as Case5, but emissions in WC are maintained at 2010s levels.	SSP2-4.5 BCMM, 2060-2064
Case9	Same as Case3, but with 20% reduction in emissions for all species.	SSP2-4.5 BCMM, 2060-2064
Case10	Same as Case1, but with 20% reduction in emissions for all species.	SSP2-4.5 BCMM, 2060-2064
Case11	Same as Case2, but with 20% reduction in emissions for all species.	SSP5-8.5 BCMM, 2060-2064
Case12	Same as Case5, but with 20% reduction in emissions for all species.	SSP2-4.5 BCMM, 2060-2064

1290

1291

1292

1293 **Table 2 The normalized mean bias (NMB), normalized mean error (NME) and the**
1294 **correlation coefficient (R) between the simulated and observed annual Nr**
1295 **deposition. Dry and wet Nr deposition fluxes of oxidized nitrogen (OXN) and**
1296 **reduced nitrogen (RDN) averaged over 2010-2014 were evaluated separately.**

	OXN_DDEP	OXN_WDEP	RDN_DDEP	RDN_WDEP
NMB (%)	-9.07	-15.12	-28.76	-17.86
NME (%)	34.76	43.24	47.17	41.72
R(temporal)	0.63	0.65	0.65	0.82
R(spatial)	0.73	0.72	0.83	0.69

1297 Note: OXN_DDEP and OXN_WDEP indicate the dry and wet deposition of oxidized nitrogen,
1298 respectively. RDN_DDEP and RDN_WDEP indicate the dry and wet deposition of reduced nitrogen,
1299 respectively.

1300

1301 **Table 3 Simulated atmospheric Nr deposition fluxes (kg N ha⁻¹ yr⁻¹) in China**
 1302 **averaged over 2010-2014 and 2060-2064 under different SSP-RCP pathways.**

Periods	Species	Dry	Wet	Total
2010-2014 (Case 1)	OXN	3.7	3.4	7.1
	RDN	3.0	4.6	7.6
	OXN + RDN	6.7	8.0	14.7
2060-2064 under SSP2-4.5 (Case 2)	OXN	1.5	1.6	3.1
	RDN	2.9	3.0	5.9
	OXN + RDN	4.4	4.6	9.0
2060-2064 under SSP5-8.5 (Case 3)	OXN	4.0	4.4	8.4
	RDN	2.9	4.1	7.0
	OXN + RDN	6.9	8.5	15.4

1303

1304

1305 **Table 4 Simulated domain-averaged OXN deposition fluxes (kg N ha⁻¹ yr⁻¹) over**
1306 **EC for cases where emissions change to 2060s levels in all regions as well as cases**
1307 **where emissions in WC are maintained at 2010s levels. Relative changes (%) are**
1308 **calculated by comparing cases with 2060s emission levels in all regions to cases**
1309 **with 2010s emission levels in WC, then dividing the difference by the 2010s**
1310 **emission levels in WC.**

	Emissions in WC are maintained at 2010s levels	Emissions change to 2060s levels in all regions	Relative change
“Baseline”	13.29 (Case7)	13.59 (Case2)	2%
“Current-goal”	5.36 (Case6)	5.08 (Case1)	-6%
“Neutral-goal”	1.90 (Case8)	1.39 (Case5)	-27%

1311

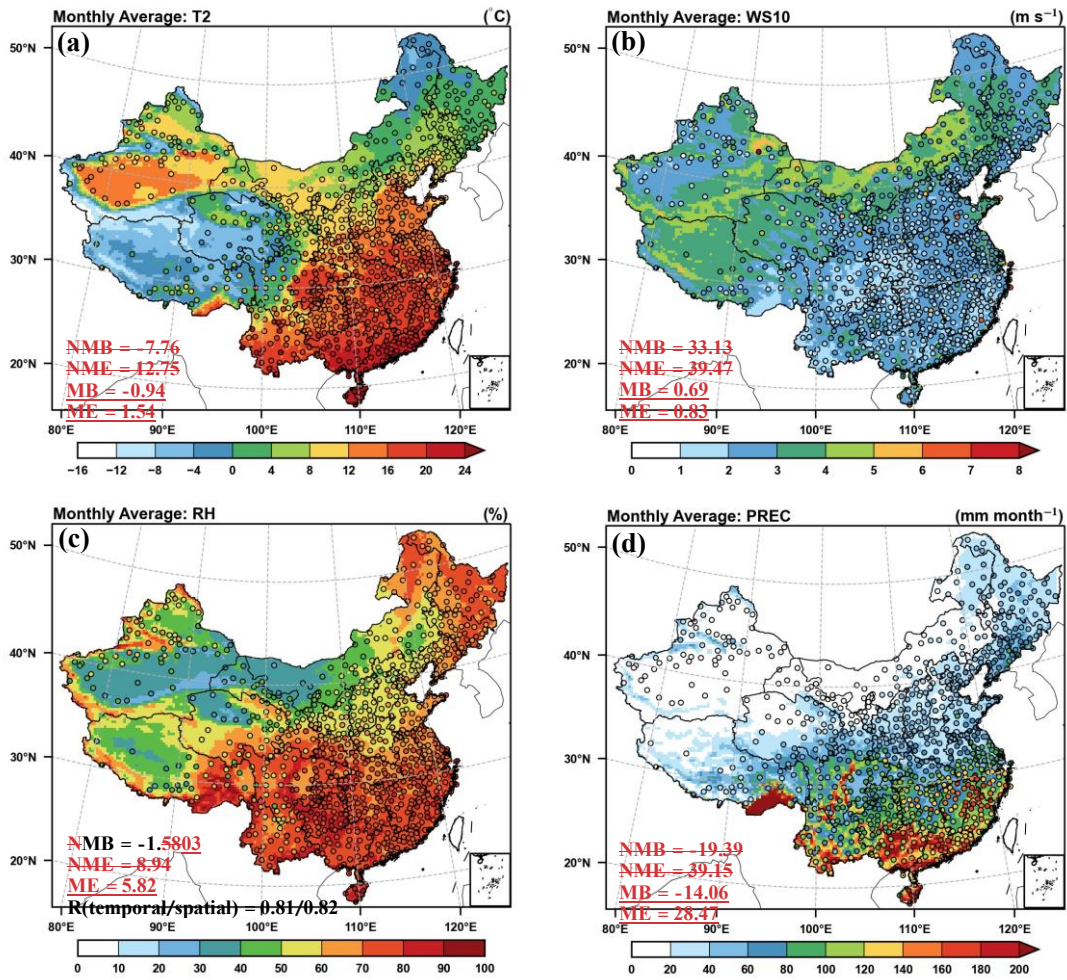
1312

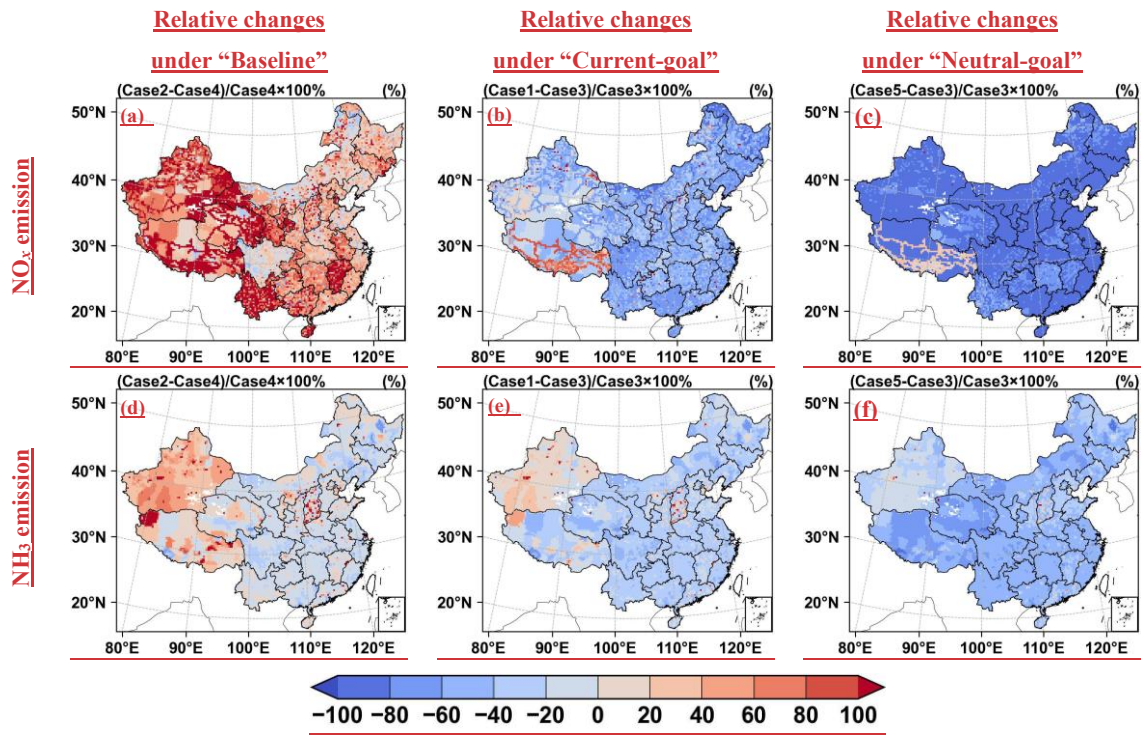
1313

1314 **Table 5 Regional average responses (%) of OXN or RDN deposition to a 20%**
 1315 **emission reduction in 2010s and 2060s under different emission scenarios over NC**
 1316 **and SC and the whole of mainland China.**

	NC	SC	China
Responses (%) of OXN deposition to NO_x emissions			
2010s	82.60	96.19	82.71
2060s under “Baseline”	83.95	92.54	88.41
2060s under “Current-goal”	91.86	103.00	81.17
2060s under “Neutral-goal”	94.59	98.07	68.83
Responses (%) of RDN deposition to NH₃ emissions			
2010s	103.11	97.63	96.30
2060s under “Baseline”	104.67	98.42	98.05
2060s under “Current-goal”	100.70	95.99	94.38
2060s under “Neutral-goal”	97.12	95.47	92.44

1317

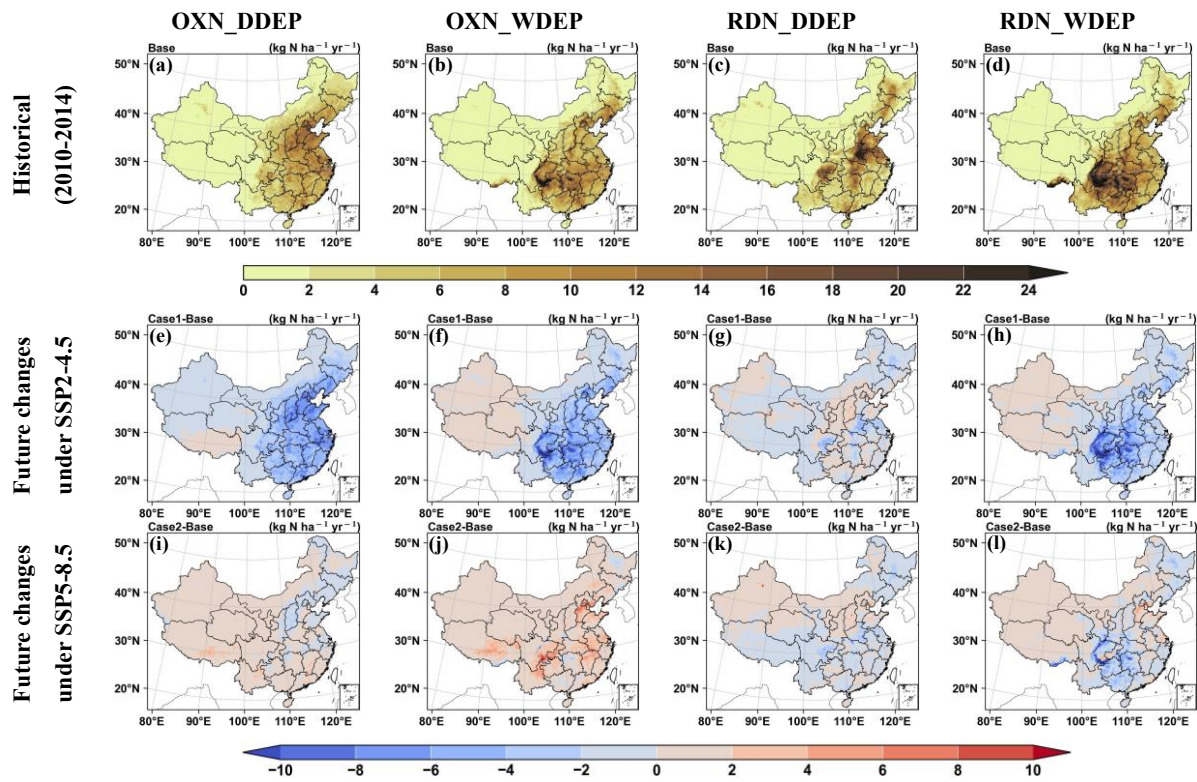




1321

1322

Figure 3



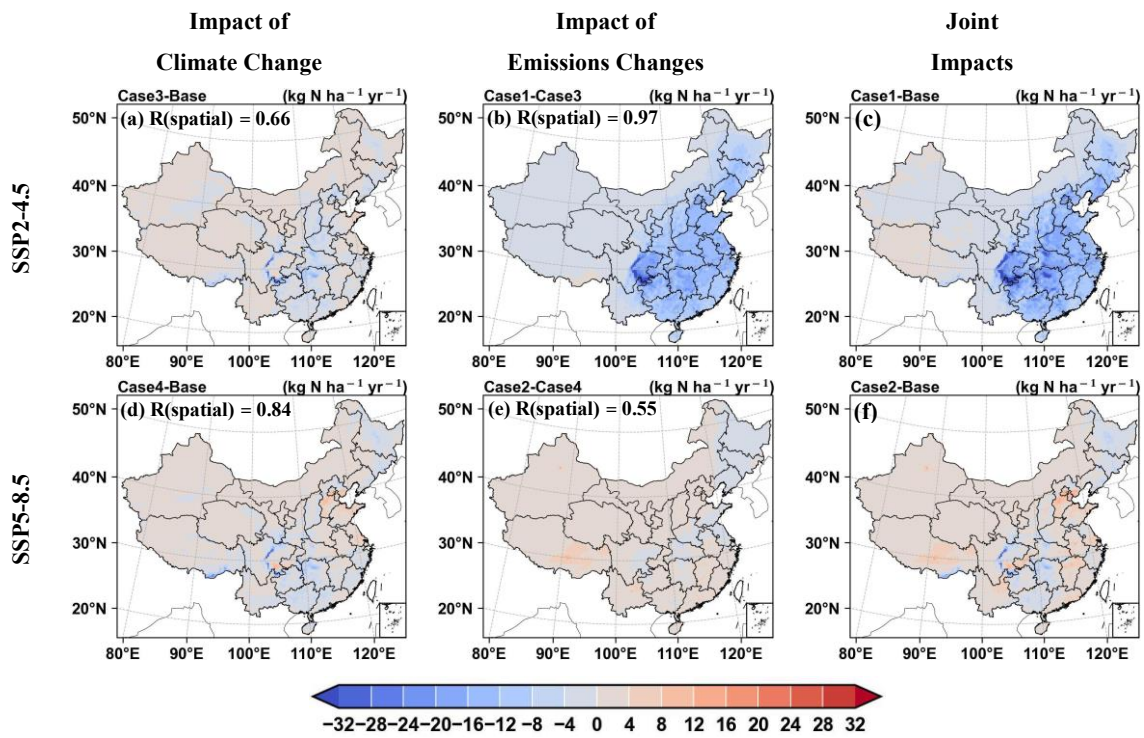
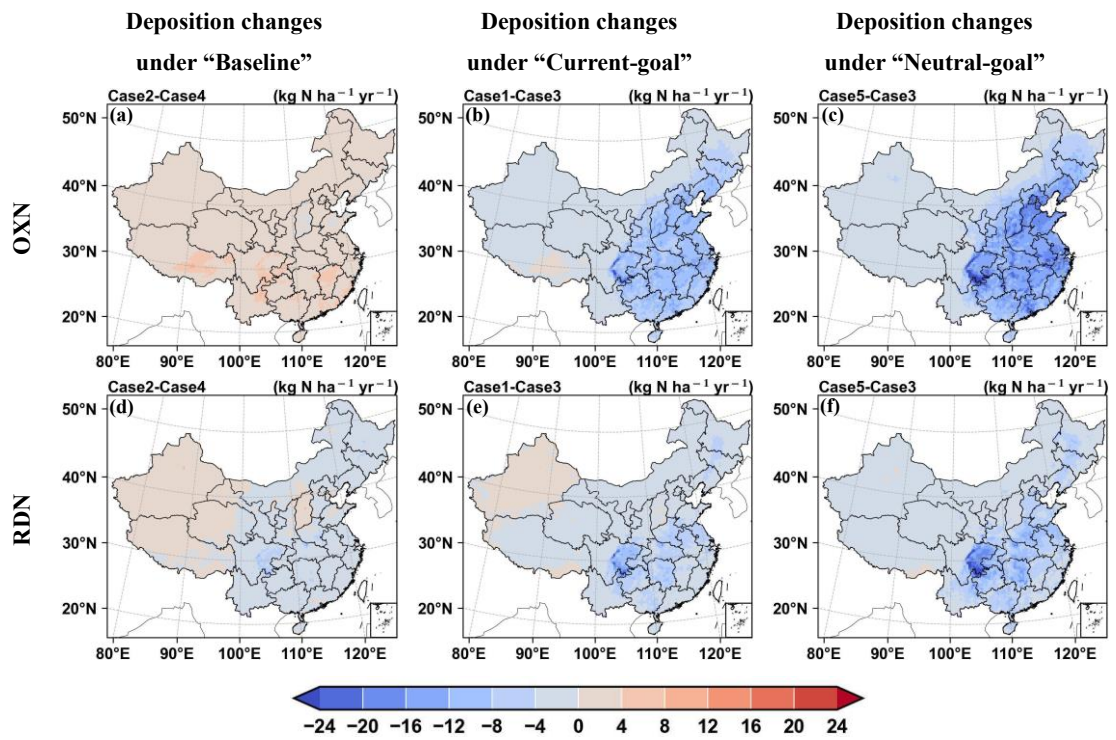


Figure 45

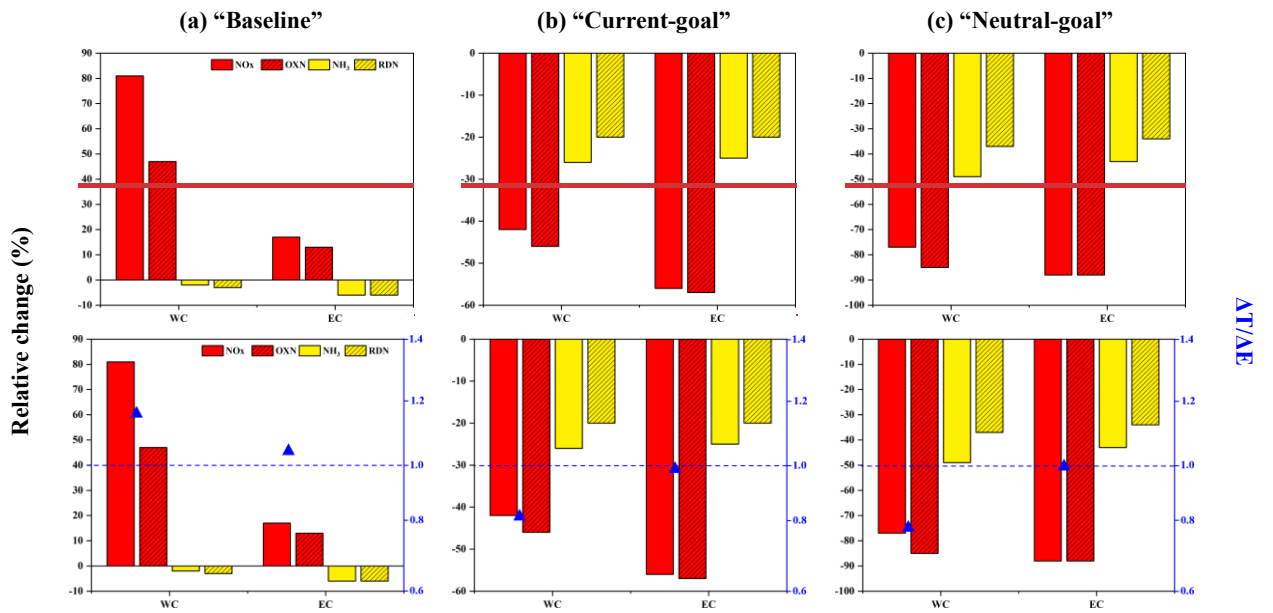


1329

1330

Figure 56

1331



1332

1333

